CALIFORNIA PATH PROGRAM
INSTITUTE OF TRANSPORTATION STUDIES
UNIVERSITY OF CALIFORNIA, BERKELEY

Magnetometer/GPS/INS Demo 2002 Support and Mitigation of GPS Signal Blockage Research

Jay Farrell
University of California Riverside

California PATH Research Report
UCB-ITS-PRR-2004-17

This work was performed as part of the California PATH Program of the University of California, in cooperation with the State of California Business, Transportation, and Housing Agency, Department of Transportation; and the United States Department of Transportation, Federal Highway Administration.

Final Report for Task Order 4232

May 2004

ISSN 1055-1425

Magnetometer/GPS/INS Demo 2002 Support and Mitigation of GPS Signal Blockage Research

Final Report

Principal Investigator: Jay Farrell
Department of Electrical Engineering
University of California, Riverside
farrell@ee.ucr.edu

March 13, 2004

Executive Summary

This project is concerned with accurately and reliably determining the state of a vehicle relative to a specified trajectory (e.g., a lane centerline). We are utilizing inertial navigation methods based on inexpensive solid state inertial sensors aided by external sensors such as carrier phase differential GPS, magnetometers, and roadway height. Due to this integration of sensors, reliability is increased relative to a single sensor approach and the changes required to the roadway infrastructure may be significantly decreased.

This projects objectives included preparation for and participation in DEMO2002, research into INS aided GPS tracking of satellites, and research into methods to use auxiliary sensors (roadway height or magnetometers) to aid the integer resolution process.

This project has been very interesting and successful. Although Demo2002 was ultimately cancelled our preparations for it were fruitful and we did participate in a smaller project demonstration with PATH at Crows Landing. In preparing for participation in Demo2002, we constructed much more robust prototypes of our GPS aided INS hardware. This include significant software re-writing that improved the reliability of the software. Overall, the hardware and software are now much more reliable and easier to use and install on test vehicles. In the area of INS aiding of a GPS receiver, research was performed and a new algorithm was design, but not implemented. We expect that this approach would lead to better satellite tracking during brief interruptions of the satellite signal. Implementation would require extensive interactions with the receiver design team, which is no longer possible due to changes in the GPS industry. In the area of aided integer ambiguity resolution, we have developed new algorithms to use information from non-GPS sensors to facilitate and speed-up the process of integer ambiguity resolution. This algorithm was evaluated in two experiments at UCR with significant improvements in the ability to correctly identify the integer ambiguities in a single epoch with fewer than 6 satellites. This algorithm was also used during the Crows Landing testing. Finally, UCR and PATH worked at PATH and Crows Landing and generated an impressive set of data as shown in Figures 12–25 of Section 4.2. This set of experiments was the culmination of the project. The experiments mounted the GPS/INS hardware on a bus that already was instrumented with the magnetometer hardware. We demonstrated that (1) the INS control state and magnetometer control state matched very well both when only the DCPGPS is aiding the INS and when both the magnetometer and DCPGPS are aiding the INS; (2) seamless transitions between magnetometer control, INS control, and manual control; (3) advanced maneuvers such as lane changes.

Contents

1 Project Introduction

Automated vehicle position control systems require both a means for determining vehicle position and a means for controlling the vehicle position [13, 32]. The vehicle position may be determined in either local (e.g., position relative to a nearby known point) or global (e.g., latitude, longitude, altitude) coordinates. A vehicle control system is then designed to maneuver the vehicle along a specified trajectory in the specified coordinate system. A variety of reference positioning systems may be considered: embedded wires [5, 12, 13], embedded magnets [32, 39], radar [13, 27], vision [6, 7, 18, 24, 28, 31, 35], and differential global positioning system (DGPS) aided inertial navigation systems (INS) [8, 9, 10, 11]. In a comparison of these alternative systems, the following factors should be considered [2]:

Infrastructure Requirements. How much does the current infrastructure have to be changed to allow use of the position referencing system? How much will maintenance of the position referencing system cost?

Reliability. Do multiple vehicles operating within the reference system suffer from interference? Does the referencing system allow for detection of faults? Does it allow for graceful degradation? Can the reference system reliably function in all weather conditions?

Performance. Can the referencing system measure position accurately enough to satisfy both tracking and comfort specifications? Does the reference system allow the previewing capability [15] necessary for satisfactory control system performance? Is the navigation system reliable enough in both nominal and emergency situations for successful commercialization?

Multipurpose. To enhance the perceived user utility, is the referencing system suitable for multiple purposes, such as lateral control, longitudinal control, lane departure warning, and ATMIS?

Implementation. Does the system allow for phased implementation? Is normal traffic hampered during implementation? How flexible is the system in its ability to accommodate temporary route changes as required to avoid detours, road maintenance, and construction?

Of particular interest to this project is the interplay of these factors when an integrated navigation system using multiple sensors is implemented. Previous research by PATH and UCR (with PATH funding) has resulted in an integrated magnetometer and GPS aided INS, which was demonstrated in automobile lateral control experiments on several occasions [11, 36, 37]. The benefits of this integrated magnetometer and GPS aided INS navigation system are as follows:

High accuracy. The magnetometer and GPS aided INS have been shown to provide position accuracy of better than 2.5 cm. This accuracy is independent of vehicle speed.

Rich State Information. The integrated navigation system provides the full vehicle state (e.g., position, velocity, attitude), inertial measurements (e.g., acceleration, angular rates), and trajectory information (e.g., arclength along the trajectory, radius of curvature, and heading versus arclength). This information not only allows improved control in normal operation, but may be necessary in more demanding emergency situations.

High-Sample Rate. The integrated navigation system currently provides vehicle state estimates at 150 Hz. Higher sample rates enable better vehicle control. In addition, the sample rate of the integrated system is independent of vehicle velocity.

Triple Redundancy. Safe vehicle operation requires the ability to detect, isolate, and accommodate sensor failures. No single sensing system will be capable of providing the integrity necessary for reliable vehicle control over a highway system because sensor faults cannot be reliably accommodated. Reliable sensor fault isolation requires at least triplicate redundancy, which is achieved by the magnetometer and GPS aided INS.

Preview Information - The integrated magnetometer and GPS aided INS provides the global vehicle position, allowing reliable access to high fidelity trajectory information (curvature, super-elevation, velocity profiles, entrance/exit trajectories, etc.) to be stored and previewed by the control law.

Reduced Infrastructure Cost. In the integrated magnetometer and GPS aided INS, trajectory relative control information can be determined by various combinations of the sensors. Therefore, for certain regions of the highway system it will be possible to increase the magnet spacing (i.e., reduce the number of magnets used per mile) thus reducing infrastructure installation and maintenance costs.

Range Independence. The accuracy of vehicle state information determined by the integrated navigation system is independent of the off-track distance. This will greatly increase the reliability of emergency maneuvers and the freedom to perform advanced maneuvers (lane changing, AHS entry and exit, platoon merging, etc.), since the integrated magnetometer and GPS aided INS allows such maneuvers to be performed in closed loop.

2 Project Scope and Objectives

The magnetometer and GPS aided INS developed under previous PATH projects [9, 10, 11] served as the starting point for this research project. The originally proposed objectives of this project were to participate in Demo 2002 and to design, develop, and evaluate algorithms to address the issue of GPS signal loss following temporary signal blockages (e.g., tunnels, overpasses). Since Demo 2002 was ultimately canceled, the first objective was revised, in consultation with PATH and Caltrans, to performing extensive testing and demonstrations onboard a bus at PATH and Crows Landing. Results from those tests are contained in Section 4.2. The second objective is important as it addresses one of the last remaining technical issues of the integrated navigation system approach - rapid reacquisition of GPS carrier phase lock and integer ambiguities following temporary loss of the GPS signal (e.g., due to tunnels). The technical details of this problem are defined in Section 3.

3 Methodology

We will investigate two possible methods for solving the problem of rapidly reacquiring phase lock and integer ambiguities following temporary GPS signal loss. The first approach is to augment the GPS measurements with auxiliary measurements (altitude or magnetometer measurements) to perform aided integer ambiguity. The second approach is to feed the INS velocity and acceleration data back into the GPS receiver to aid the receiver tracking loops. This aiding would allow the receiver phase tracking loop bandwidth to be deceased significantly so that the receiver could maintain lock during longer periods of temporary loss of the GPS signal.

3.1 Measurements

In this section we will be concerned with measurements from a GPS receiver, distance measurements relative to a trajectory from a magnetometer, and altitude measurements from stored trajectory information. A measurement of a variable will be indicated by a tilde '~' over the variable. This section derives the error model for each measurement.

3.1.1 Code and Carrier Phase Measurements

The L1 and L2 code and carrier phase measurements of each satellite can be modeled as

$$\begin{aligned}
\tilde{\rho_1} &= R + c\Delta t_r + c\Delta t_{sv} + \frac{f_2}{f_1} I_a + E_{cm} + MP_1 + \eta_1 \\
\tilde{\rho_2} &= R + c\Delta t_r + c\Delta t_{sv} + \frac{f_1}{f_2} I_a + E_{cm} + MP_2 + \eta_2 \\
\tilde{\phi_1}\lambda_1 &= R + c\Delta t_r + c\Delta t_{sv} - \frac{f_2}{f_1} I_a + E_{cm} + mp_1 - N_1\lambda_1 + n_1 \\
\tilde{\phi_2}\lambda_2 &= R + c\Delta t_r + c\Delta t_{sv} - \frac{f_1}{f_2} I_a + E_{cm} + mp_2 - N_2\lambda_1 + n_2
\end{aligned}$$

where $R = \|X_{sv} - X_a\|$ is the geometric distance between the satellite position X_{sv} and receiver antenna position X_a, $c\Delta t_r$ is receiver clock bias, $c\Delta t_{sv}$ is the satellite clock bias. Satellite clock bias can be partially compensated by ephemeris data. E_{cm} represents common errors other than dispersive effects such as ionosphere and I_a represents dispersive effects such as ionospheric error. E_{cm} and I_a can be eliminated by differential operations. The uncorrected error I_a between rover and base should be small if the distance between rover and base is small. So after DGPS corrections, only multipath and receiver measurement errors are left. The quantities N_1 and N_2 are unknown integer ambiguities. One of the goals of this research is to identify the integer ambiguities for each satellite.

The single differenced measurements between a base and rover can be represented as

$$\nabla\rho_1 = R + c\Delta t_r + \frac{f_2}{f_1}\delta I_a + MP_1 + \eta_1 \tag{1}$$

$$\nabla\rho_2 = R + c\Delta t_r + \frac{f_1}{f_2}\delta I_a + MP_2 + \eta_2 \tag{2}$$

$$\nabla\phi_1\lambda_1 = R + c\Delta t_r - \frac{f_2}{f_1}\delta I_a - N_1\lambda_1 + mp_1 + n_1 \tag{3}$$

$$\nabla\phi_2\lambda_2 = R + c\Delta t_r - \frac{f_1}{f_2}\delta I_a - N_2\lambda_2 + mp_2 + n_2 \tag{4}$$

where δI_a is the residual ionospheric error that is not canceled in the DGPS operation. Combining eqn. (1) and eqn. (2) yields the narrow code measurement [19]:

$$\left(\frac{\nabla\rho_1}{\lambda_1} + \frac{\nabla\rho_2}{\lambda_2}\right)\lambda_n = R + c\Delta t_r + \delta I_a + \frac{\lambda_n}{\lambda_1}(MP_1 + \eta_1) + \frac{\lambda_n}{\lambda_2}(MP_2 + \eta_2). \tag{5}$$

Combining eqn. (3) and eqn. (4) yields the wide phase measurement:

$$\begin{aligned}\nabla\Phi_w &= (\nabla\phi_1 - \nabla\phi_2)\lambda_w + (N_1 - N_2)\lambda_w \\ &= R + c\Delta t_r + \delta I_a + \frac{\lambda_w}{\lambda_1}(mp_1 + n_1) - \frac{\lambda_w}{\lambda_2}(mp_2 + n_2).\end{aligned} \tag{6}$$

Subtracting eqn. (5) from eqn. (6) and rearranging yields:

$$\begin{aligned}\left(\frac{\nabla\rho_1}{\lambda_1} + \frac{\nabla\rho_2}{\lambda_2}\right)\lambda_n - (\nabla\phi_1 - \nabla\phi_2)\lambda_w &= (N_1 - N_2)\lambda_w + \frac{\lambda_n}{\lambda_1}(MP_1 + \eta_1) + \frac{\lambda_n}{\lambda_2}(MP_2 + \eta_2) \\ &\quad - \frac{\lambda_w}{\lambda_1}(mp_1 + n_1) + \frac{\lambda_w}{\lambda_2}(mp_2 + n_2).\end{aligned} \tag{7}$$

Therefore, an initial estimate of the wide lane integer $N_w = N_1 - N_2$ can be obtained based on eqn. (7) since all quantities in the left hand side are available by measurement. This initial estimate is not necessarily correct, due to the various error terms in the right hand side, but it does provide a starting point for a local search.

3.1.2 Altitude

The INS is calculating the vehicle position in global coordinates. The system includes a model of the roadway that is a curve fit to the lane centerline. This curve fit models the latitude, longitude, and geodetic altitude of the centerline as a function of arclength along the trajectory. When calculating the control state, the system finds the point on the trajectory that is nearest to the vehicle location. Therefore, the altitude of the lane centerline is known. The height of the vehicle is a quantity that is known in advance. Therefore, the height of the navigation system on top of the vehicle is easily computed at any location in the vicinity of the lane trajectory. The sum of the roadway height and the vehicle height (after appropriate translations) will be referred to as the measured altitude $\tilde{a}(X_o)$. The measured altitude is modeled as

$$\tilde{a} = a(X) + n_a \tag{8}$$

where $a(X)$ is the true altitude at location X and n_a represents measurement 'noise'. The altitude measurement noise comes from several sources: error in the trajectory fitting process, error in the data used as inputs to the trajectory fit process, and the fact that the altitude at X may be different from the altitude of the nearest point on the trajectory. The standard deviation of all these combined errors is expected to be less than 5 cm.

3.1.3 Magnetometer

The magnetometer system provides a measurement of the trajectory relative distance that is accurate to about 1.0 cm. The magnetometer measurement is modeled as

$$\tilde{d} = d(X) + n_d \tag{9}$$

where n_d has standard deviation of 1.0 cm.

3.2 Calculated Values for Measurements

In the sections that follow, measurement residuals and linearized measurement equations will be used both for the position solution and for the integer ambiguity resolution process. These methods are based on the Taylor expansion:

$$f(X) = f(X_o) + H\,(X - X_o) + h.o.t.'s \tag{10}$$

where X_o is the linearization point, $H = \left.\frac{\partial f(X)}{\partial X}\right|_{X=X_o}$ is a row vector, $h.o.t.'s$ represent higher order terms that will be dropped, and $\delta X = (X - X_o)$. Given expression (10), the residual measurement is formed as

$$\tilde{f}(X) - \hat{f}(X_o) = H\ \delta X + n \tag{11}$$

where $\tilde{f}$ is the measured value and $\hat{f}(X_o)$ is the calculated value at X_o. If it is possible to estimate δX from a set of measurements, then the estimate of X can be corrected as $\hat{X} = X_o + \delta\hat{X}$. Although this process introduces error through the neglected higher order terms, the linear relationship between the residual measurements and the variable δX greatly simplifies the process of using the measurements.

To complete this subsection, we must specify the equations that are used to compute the code pseudorange, phase pseudorange, altitude, and magnetometer estimates based when we have a prior location estimate X_o in ECEF coordinates. The computation of the code pseudorange to satellite i in meters is

$$\hat{\rho}_i(X_o) = \|X_{sv_i} - X_o\| + c\Delta t_r. \tag{12}$$

Therefore, the residual pseudorange is

$$\Delta\rho_i = \tilde{\rho}_i - \hat{\rho}_i(X_o) = h_{ix}\delta x + h_{iy}\delta y + h_{iz}\delta z + \delta c t_r + \epsilon_i \tag{13}$$

where ϵ_i is the cumulative noise (e.g., multipath, h.o.t.'s, receiver noise) and as described in [8] and [23] the h_{ix}, h_{iy} and h_{iz} terms are the direction cosines of the unit vector pointing from X_o to the ith satellite. The computation of the phase pseudorange to satellite i in cycles is

$$\hat{\phi}_i(X_o) = \left(\|X_{sv_i} - X_o\| + c\Delta t_r\right)\frac{1}{\lambda}. \tag{14}$$

Therefore, the residual phase measurement is

$$\Delta\phi_i\lambda = \left(\tilde{\phi}_i - \hat{\phi}_i(X_o)\right)\lambda = h_{ix}\delta x + h_{iy}\delta y + h_{iz}\delta z + \delta c t_r - N_i\lambda + \epsilon_i. \tag{15}$$

The computed altitude is the third coordinate of X_o when represented in tangent frame,

$$\hat{a}(X_o) = D_o, \text{ where } \begin{bmatrix} N_o \\ E_o \\ D_o \end{bmatrix} = \mathbf{R}_{e2t}\left(X_o - \mathbf{X}_0\right), \tag{16}$$

where $\mathbf{X}_0$ is the origin of the tangent frame in ECEF coordinates, and R_{e2t} is the rotation matrix from ECEF to tangent frame. The residual altitude measurement is

$$\Delta a = \tilde{a} - \hat{a} = \frac{\partial a}{\partial x}\delta x + \frac{\partial a}{\partial y}\delta y + \frac{\partial a}{\partial z}\delta z + \xi, \tag{17}$$

where

$$\begin{bmatrix} \frac{\partial a}{\partial x} & \frac{\partial a}{\partial y} & \frac{\partial a}{\partial z} \end{bmatrix} = \begin{bmatrix} 0 & 0 & 1 \end{bmatrix}\mathbf{R}_{e2t}. \tag{18}$$

The computed distance from the trajectory is

$$\hat{d} = \mathbf{K}^T \mathbf{R}_{e2t} \left(X_o - X_T \right) \tag{19}$$

where $\mathbf{K}$ is the normal to the trajectory that lies in the tangent plane and X_T is the point on the trajectory closest to X_o. Therefore, the residual magnetometer measurement is

$$\Delta d = \frac{\partial d}{\partial x}\delta x + \frac{\partial d}{\partial y}\delta y + \frac{\partial d}{\partial z}\delta z + \epsilon_d \tag{20}$$

where

$$\left[\begin{array}{ccc} \frac{\partial d}{\partial x} & \frac{\partial d}{\partial y} & \frac{\partial d}{\partial z} \end{array} \right] = \mathbf{K}^T \mathbf{R}_{e2t}. \tag{21}$$

The residual measurements described in this section are now used as aiding signals in the aided INS that is implemented. The following sections will discuss the position solution, without INS, using these residual measurements. It is presented in this fashion as it is this position solution that is relevant to the integer ambiguity resolution problem.

3.3 Position Solution

In this section, we will consider an aided GPS position solution. The aiding signals that we consider are altitude, magnetometer or both. The approach described below is valid when either one or both aiding signals are used. The aiding signal is denoted by ψ.

Given the aiding measurement ψ and n code pseudorange measurements, all the measurements can be put in the matrix form

$$\delta \mathbf{Y} = \mathbf{H}\ \delta \mathbf{X} \tag{22}$$

by making the definitions $\delta \mathbf{Y} = \left[\begin{array}{c} \Delta\rho_1 \\ \Delta\rho_2 \\ \vdots \\ \Delta\rho_n \\ \Delta\psi \end{array} \right]$, $\delta \mathbf{X} = \left[\begin{array}{c} \delta x \\ \delta y \\ \delta z \\ \delta c t_r \end{array} \right]$, and $\mathbf{H} = \left[\begin{array}{cccc} h_{1x} & h_{1y} & h_{1z} & 1 \\ h_{2x} & h_{2y} & h_{2z} & 1 \\ & \vdots & & \\ h_{nx} & h_{ny} & h_{nz} & 1 \\ \frac{\partial \psi}{\partial x} & \frac{\partial \psi}{\partial y} & \frac{\partial \psi}{\partial z} & 0 \end{array} \right]$.

The aided differential pseudorange position solution is

$$\delta \mathbf{X} = \left[\mathbf{H^T W^{-1} H} \right]^{-1} \mathbf{H^T W^{-1}} \delta \mathbf{Y} \tag{23}$$

where $\mathbf{W}$ is a weighting matrix which assigns different weights to the measurements according to their noise levels.

3.4 Residual Matrix S and its Properties

Given $\delta \mathbf{X}$, the error of the pseudorange residual vector is

$$\begin{aligned} \mathbf{r} &= \delta \mathbf{Y} - \mathbf{H} \delta \mathbf{X} \\ &= (\mathbf{I} - \mathbf{H} \left[\mathbf{H^T W^{-1} H} \right]^{-1} \mathbf{H^T W^{-1}}) \delta \mathbf{Y} \\ &= \mathbf{S} \delta \mathbf{Y} \end{aligned} \tag{24}$$

with

$$\mathbf{S} = \mathbf{I} - \mathbf{H} \left[\mathbf{H^T W^{-1} H} \right]^{-1} \mathbf{H^T W^{-1}}. \tag{25}$$

The $\mathbf{S}$ matrix is positive semidefinite and has nice properties, such as

1. $\mathbf{S}$ is idempotent: $\mathbf{S} = \mathbf{S^2} = \mathbf{S^3} \cdots$;
2. $\mathbf{S}$ has rank equal to $n+1-k$ where k is the dimension of $\delta \mathbf{X}$. For single differential GPS, there are four unknown parameters $(\delta x, \delta y, \delta z, \delta c t_r)$ so $k = 4$. For double differential GPS, there are three unknown parameters $(\delta x, \delta y, \delta z)$ so $k = 3$;

3. The eigenvalues of $\mathbf{S}$ are either 1 or 0.
   Therefore using the singular value decomposition, $\mathbf{S}$ can be written as

$$\mathbf{S} = \mathbf{U}\mathbf{X}\mathbf{V}^{\mathbf{T}} \tag{26}$$

   where $\mathbf{U}$ and $\mathbf{V}$ are unitary matrices,

$$\mathbf{U} = [\mathbf{u_1}\mathbf{u_2}\cdots\mathbf{u_{n+1}}] \tag{27}$$

   with

$$\mathbf{u_i}^{\mathbf{T}}\mathbf{u_i} = \mathbf{1}, \quad \mathbf{u_i}^{\mathbf{T}}\mathbf{u_j} = \mathbf{0} \quad (i \neq j) \ ;$$

$$\mathbf{X} = \begin{bmatrix} \mathbf{I}_{(n+1-k)\times(n+1-k)} & \mathbf{0}_{(n+1-k)\times k} \\ \mathbf{0}_{k\times(n+1-k)} & \mathbf{0}_{k\times k} \end{bmatrix}; \tag{28}$$

$$\mathbf{V} = [\mathbf{v_1}\mathbf{v_2}\cdots\mathbf{v_{n+1}}] \tag{29}$$

   with

$$\mathbf{v_i}^{\mathbf{T}}\mathbf{v_i} = \mathbf{1}, \quad \mathbf{v_i}^{\mathbf{T}}\mathbf{v_j} = \mathbf{0} \quad (i \neq j) \ .$$

The $\mathbf{S}$ matrix and its special properties will be useful in the process of estimating the integer ambiguities.

3.5 Aided Integer Ambiguity Resolution

Real time precise positioning with GPS requires carrier phase intetger ambiguity resolution. After resolving the ambiguities, N_1 and N_2 in eqns. (3–4), the carrier phase observables can be used as very precise range measurements. With these precise ranges, positioning accuracies at the cm or even mm level can be obtained. Many efforts have been devoted to solve the ambiguity problem. Basically there are three classes of ambiguity resolution techniques [17]: (1) ambiguity resolution in measurement space [15, 19, 20, 29]; (2) ambiguity resolution in position space [4, 26, 30]; (3) ambiguity resolution in ambiguity space [1, 14, 21, 22, 25, 34]. Ambiguity resolution in measurement space is also referred as geometry independent resolution. It starts with smoothed code for wide lane ambiguity resolution. It then steps to L1, L2, and narrow lane integers from the integer resolved wide-lane phase ranges. The success of this method depends upon the accuracy of the smoothed code measurements which may take a long time. Ambiguity resolution in position space was originally developed by Counselman. In this method, the initial baseline is required to be sufficiently accurate. Intensive computation stops it from being widely used. Ambiguity space approaches attempt to find a vector of integer candidates that results in a minimum norm measurement residual. In this section, we are concerned with ambiguity space approaches aided by auxiliary (non-GPS) measurements. Many variations of ambiguity space techniques have been proposed to minimize the computational requirements per epoch and to minimize the number of epochs of data required for a reliable solution. Yang [38] developed an efficient and reliable search technique in the ambiguity domain. Sinko [33] suggested an altitude aiding ambiguity resolution algorithm using a least squares methodology. In the paper [3] and this section, we extend the approach of Yang to work with auxiliary (aiding) measurements. Two sets of experimental results are included. The test results show that the aided integer ambiguity resolution approach finds the correct integers above 90% of the time even when there are as few as five satellites available.

Starting from eqn. (15), if the integer ambiguity for each satellite were known, a process similar to that of Section 3.3 could be used to estimate the position based on the phase measurements. Moving the integer to the left hand side yields the differential phase measurement is

$$(\Delta\mathbf{\Phi} + \mathbf{N})\,\lambda = h_x\delta x + h_y\delta y + h_z\delta z + \delta c t_r + \epsilon \tag{30}$$

where $\Delta\mathbf{\Phi}$ is the vector of residual phase measurements $\Delta\mathbf{\Phi}^T = [\Delta\phi_1, \Delta\phi_2, \cdots, \Delta\phi_n]$ and $\mathbf{N}$ is the vector of integer ambiguities $\mathbf{N}^T = [N1, N_2, \cdots, N_n]$. Combining the phase and aiding sensor residual measurements yields

$$\delta\mathbf{Y} = \mathbf{H}\delta\mathbf{X} \tag{31}$$

where $\delta\mathbf{Y} = \left[\begin{array}{l} (\Delta\mathbf{\Phi} + \mathbf{N})\,\lambda \\ \Delta\psi \end{array} \right]_{(n+1)\times 1}$ and $\mathbf{H}$ and $\delta\mathbf{X}$ are defined in Section 3.3.

Since $\mathbf{N}$ is not known, we let $\mathbf{N} = \mathbf{N}^o + \delta\mathbf{N}$ where $\mathbf{N}^o$ is a nominal vector of integers which is near the correct integer ambiguity vector (e.g, estimated by eqn. (7)) and $\delta\mathbf{N}$ is a vector of perturbation integers. Then we can write

$$\delta\mathbf{\Phi}(\delta\mathbf{N}) = \delta\mathbf{\Phi}^o + \delta\mathbf{N}\lambda \tag{32}$$

where $\delta\mathbf{\Phi}^o = (\Delta\mathbf{\Phi} + \mathbf{N}^o)\,\lambda$. Then combining the phase measurements with the aiding sensor for the assumed integer perturbation, the estimated position as a function of the integer perturbation candidate $\delta\mathbf{N}$ is

$$\delta\mathbf{X}(\delta\mathbf{N}) = \left[\mathbf{H^T W^{-1} H}\right]^{-1}\mathbf{H^T W^{-1}}\delta\mathbf{Y}(\delta\mathbf{N}) \tag{33}$$

where

$$\begin{aligned} \delta\mathbf{Y}(\delta\mathbf{N}) &= \left[\begin{array}{l} (\delta\mathbf{\Phi}^o + \delta\mathbf{N}\lambda) \\ \Delta\psi \end{array} \right]_{(n+1)\times 1} \\ &= \mathbf{Y}^o + \mathbf{\Delta N}\lambda \end{aligned}$$

where $\mathbf{Y}^o = \left[\begin{array}{l} \delta\mathbf{\Phi}^o \\ \Delta\psi \end{array} \right]$ and $\mathbf{\Delta N} = \left[\begin{array}{l} \delta\mathbf{N} \\ 0 \end{array} \right]$. The argument $\delta\mathbf{N}$ is explicitly specified to emphasize the fact that the estimated position is a function of the assumed integer perturbation vector. The aided phase residual vector resulting for $\delta\mathbf{N}$ is

$$\begin{aligned} \mathbf{r}(\delta\mathbf{N}) &= \mathbf{S}\delta\mathbf{Y}(\delta\mathbf{N}) && (34)\\ &= \mathbf{S}\mathbf{Y}^o + \mathbf{S\Delta N}\lambda && (35)\\ &= \mathbf{r}^o + \mathbf{S\Delta N}\lambda && (36) \end{aligned}$$

where $\mathbf{r}^o = \mathbf{S}\mathbf{Y}^o$ and $\mathbf{S}$ is defined in eqn. (25). The objective of the integer resolution process is to choose an integer vector $\mathbf{\Delta N}$ to minimize the two norm of $\mathbf{r}(\delta\mathbf{N})$. The constraint that the perturbation must be integer makes this a nonlinear problem.

3.5.1 Reduction of searching space

The best real valued solution is

$$\mathbf{r_0} + \mathbf{S\Delta N}\lambda = \mathbf{0} \Rightarrow \mathbf{S\Delta N} = -\mathbf{r_0}/\lambda. \tag{37}$$

Replacing $\mathbf{S}$ with eqn. (26), we have

$$\begin{aligned} &\mathbf{U}\mathbf{X}\mathbf{V}^T\mathbf{\Delta N} = -\mathbf{r_0}/\lambda \\ \Leftrightarrow\ &\mathbf{X}\mathbf{V}^T\mathbf{\Delta N} = -\mathbf{U}^T\mathbf{r_0}/\lambda = \mathbf{r_1} \\ \Leftrightarrow\ &\left[\begin{array}{l} \mathbf{v}_1^T \\ \vdots \\ \mathbf{v}_{(n+1-k)}^T \\ \mathbf{0}_{k\times(n+1)} \end{array} \right] \mathbf{\Delta N} = \mathbf{r_1}. \end{aligned} \tag{38}$$

The above equation can be re-written as

$$\left[\begin{array}{ll} \mathbf{A}_1 & \mathbf{A}_2 \\ \mathbf{0}_{k\times(n+1-k)} & \mathbf{0}_{k\times k} \end{array} \right] \left[\begin{array}{l} \mathbf{\Delta N}_1 \\ \mathbf{\Delta N}_2 \end{array} \right] = \left[\begin{array}{l} \mathbf{r}_{11} \\ \mathbf{r}_{12} \end{array} \right] \tag{39}$$

which for any hypothesized integer vector $\mathbf{\Delta N}_2$ allows calculation of

$$\mathbf{\Delta N}_{1f} = \mathbf{A}_1^{-1}(\mathbf{r}_{11} - \mathbf{A}_2\mathbf{\Delta N}_2) \tag{40}$$

where the integer vector is computed as

$$\mathbf{\Delta N} = round\left(\left[\begin{array}{l} \mathbf{\Delta N}_{1f} \\ \mathbf{\Delta N}_2 \end{array} \right] \right) = \left[\begin{array}{l} \mathbf{\Delta N}_1 \\ \mathbf{\Delta N}_2 \end{array} \right] \tag{41}$$

Obviously, given $\Delta\mathbf{N}_2$ we can calculate $\Delta\mathbf{N}_{1f}$ based on eqn. (40), therefore, the search space is reduced from searching all integers for n satellites to searching $\Delta\mathbf{N}_2$ for k satellites.

3.5.2 Implementation

We can develop an algorithm with lower computational requirements if we avoid the singular value decomposition. By applying Property 1 of the $\mathbf{S}$ matrix, eqn. (37) can be rewritten as

$$\mathbf{S}(\mathbf{r_0} + \mathbf{S}\boldsymbol{\Delta}\mathbf{N}\lambda) = 0 \;\Rightarrow \mathbf{S}(\boldsymbol{\Delta}\mathbf{N} + \mathbf{r_0}/\lambda) = 0. \tag{42}$$

According to the property 2 of the $\mathbf{S}$ matrix, there are only $n+1-k$ rows of the $\mathbf{S}$ matrix that are linearly independent. Rearranging the $\mathbf{S}$ matrix so that its first $n+1-k$ rows are linearly independent, eqn. (42) can be rewritten as

$$\begin{bmatrix} \mathbf{S}_{11} & \mathbf{S}_{12} \\ \mathbf{S}_{21} & \mathbf{S}_{22} \end{bmatrix} \begin{bmatrix} \boldsymbol{\Delta}\mathbf{N}_1 + \mathbf{r}_{01} \\ \boldsymbol{\Delta}\mathbf{N}_2 + \mathbf{r}_{02} \end{bmatrix} = \mathbf{0} \tag{43}$$

with $\mathbf{S}_{11} \in R^{(n+1-k)\times(n+1-k)}$, $\mathbf{S}_{12} \in R^{(n+1-k)\times k}$, $\mathbf{S}_{21} \in R^{k\times(n+1-k)}$, $\mathbf{S}_{22} \in R^{k\times k}$, $\boldsymbol{\Delta}\mathbf{N}_1 \in R^{(n+1-k)\times 1}$, $\boldsymbol{\Delta}\mathbf{N}_2 \in R^{k\times 1}$. From eqn.(43), we have

$$\mathbf{S}_{11}(\boldsymbol{\Delta}\mathbf{N}_1 + \mathbf{r}_{01}) + \mathbf{S}_{12}(\boldsymbol{\Delta}\mathbf{N}_2 + \mathbf{r}_{02}) = \mathbf{0} \tag{44}$$

$$\Rightarrow \boldsymbol{\Delta}\mathbf{N}_{1f} = -\mathbf{T}(\boldsymbol{\Delta}\mathbf{N}_2 + \mathbf{r}_{02}) - \mathbf{r}_{01} \tag{45}$$

with

$$\mathbf{T} = \mathbf{S}_{11}^{-1}\mathbf{S}_{12} \tag{46}$$

$$\Rightarrow \boldsymbol{\Delta}\mathbf{N}_1 = round(\boldsymbol{\Delta}\mathbf{N}_{1f}). \tag{47}$$

The goal of rearranging the $\mathbf{S}$ matrix is to minimize the effect of the measurement noise on the integer estimation and make $\mathbf{S}_{11}$ nonsingular. Therefore, we select $n+1-k$ measurements that minimize the diagonal values of matrix $\mathbf{S}_{11}^{-1}$.

The algorithm is implemented in our system as follows:

1. Calculate the $\mathbf{S}$ matrix based on eqn. (25). Sort the diagonal elements of $\mathbf{S}$ matrix. Rearrange $\mathbf{S}$ matrix by permutation matrices (see [16]). Split the $\mathbf{S}$ matrix as in eqn. (43). And, calculate the $\mathbf{T}$ matrix.

2. Initialize the wide integer $\mathbf{N}_{w0}$ based on eqn. (7) and calculate the initial phase range residual vector based on eqn. (36).

3. In three "for" loops, hypothesize the sequence of integer candidate vectors $\boldsymbol{\Delta}\mathbf{N}_2 = [i, j, k, 0]^T$. For each candidate, calculate $\boldsymbol{\Delta}\mathbf{N}_1$ based on eqn. (47). Save the norm of the residual vector for each candidate vector δN. Note that three "for" loops are used for the case without aiding measurements. With one aiding measurement, $k = 0$ since there is no integer ambiguity for the aiding measurement. Each aiding measurement removes one of the for loops. Therefore only two "for" loops are required with one aiding measurement.

4. Outside the loops, sort the $\boldsymbol{\Delta}\mathbf{N}$ sets according to the norm of their residuals. Use the candidate $\boldsymbol{\Delta}\mathbf{N}$ with the minimal residual and make the correction

$$\mathbf{N}_w = \mathbf{N}_{w0} + \boldsymbol{\Delta}\mathbf{N}. \tag{48}$$

5. Calculate wide phase range based on eqn. (6). Initialize the L1 integer $\mathbf{N}_{l10}$ to match wide phase range. Calculate the initial phase range residual vector based on eqn. (36).

6. Repeat step 3 and step 4 using L1 phase data and define

$$\mathbf{N}_{l1} = \mathbf{N}_{l10} + \boldsymbol{\Delta}\mathbf{N}. \tag{49}$$

7. Calculate L2 and narrowlane integers as

$$\mathbf{N}_{l2} = \mathbf{N}_{l1} - \mathbf{N}_w \tag{50}$$
$$\mathbf{N}_n = \mathbf{N}_{l1} + \mathbf{N}_{l2}. \tag{51}$$

8. Validate the integers by comparing the measurements described in Section 3.1:

$$\begin{aligned} res_{12} &= (\nabla\phi_1 + N_1)\lambda_1 - (\nabla\phi_2 + N_2)\lambda_2 \\ res_{1w} &= (\nabla\phi_1 + N_1)\lambda_1 - (\nabla\phi_w + N_w)\lambda_w \\ res_{1n} &= (\nabla\phi_1 + N_1)\lambda_1 - (\nabla\phi_1 + \nabla\phi_2 + N_1 + N_2)\lambda_n \end{aligned}$$

These residuals can be analyzed by standard hypothesis testing methods to validate whether they are correct.

Test results are shown in Section 4.2.

3.6 INS aided GPS

The performance of a GPS receiver is degraded seriously when GPS signals are intermittent or blocked out, since the number of satellite signals available for a solution is decreased. A traditional multichannel receiver does not share signal tracking information between channels and does not have auxiliary sensors available to it to help with signal tracking. Since our application includes an INS that is tracking the vehicle as it maneuvers, we should be able to improve the ability of the receiver to coast through short periods of signal loss without losing phase lock and by aiding signal reacquisition in situations where signals are lost.

INS aided GPS described herein has two modes. First, the system uses conventional code and carrier tracking loops until stable code and carrier phase measurements are achieved. Then it transitions to a ultra-tight mode where the INS aides the code and carrier tracking loops. For each channel, there is a signal quality monitor to check whether the signal is available or not. When the signal is available, the standard tracking approach is used. In the case of signal loss, the INS will feed the required tracking information to that channel. The objective of this approach is to avoid the search phase of the signal reacquisition process. When a few of the satellites drop out, the remaining satellites maintain the INS accuracy and the INS keeps the tracking channels for the missing satellites near their correct values for an extended period of time. When all the satellites drop out (e.g., going under a bridge or overpass), the INS can keep all channels near their correct values for on the order of 10 seconds, even with vehicle maneuvering. When the signals return, the channels should continue tracking with a small error transient, but without the delay involved in search and reacquisition. This allows channels with strong signals to aid channels with weak signal. It also allows new or returning signals to be tracked more quickly.

3.6.1 Traditional Approach

The generation of the code and carrier frequency and phase measurements in a receiver is performed in hardware as illustrated in Fig 1. The digital intermediate frequency (IF) signal at time t_k is expressed as:

$$s(t_k) = A\ C(t_k)\ D(t_k)\ \cos[\omega_{IF}t_k + \phi(t_k)] \tag{52}$$

where

$$\phi(t_k) = 2\pi \int_{t_o}^{t_k} f_D(\tau)d\tau \tag{53}$$

and A is the signal amplitude, $C(t_k)$ is the bipolar PRN modulation code, $D(t_k)$ is the 50bps bipolar data modulation code, ω_{IF} is the intermediate frequency, ϕ_0 is the unknown initial carrier phase at the time of lock, t_o is the initial lock time, and $f_D(t)$ is Doppler frequency. The Doppler frequency is determined predominantly by the relative motion of the satellite and receiver antennae. The carrier numerically controlled oscillator (NCO) for each channel generates the estimated carrier phase $\hat{\phi}(t_k)$ for the satellite assigned to that channel. The carrier NCO is initialized at the intermediate frequency ω_{IF}. So the output of the NCO is $\omega_{IF}t_k + \hat{\phi}(t_k)$. The in-phase (I) and quadraphase (Q) signals are produced by the mixers and can be represented as follows:

$$I(t_k) = A\ C(t_k)\ D(t_k)\ \cos[\omega_{IF}t_k + \phi(t_k)]\cos[\omega_{IF}t_k + \hat{\phi}(t_k)] \tag{54}$$

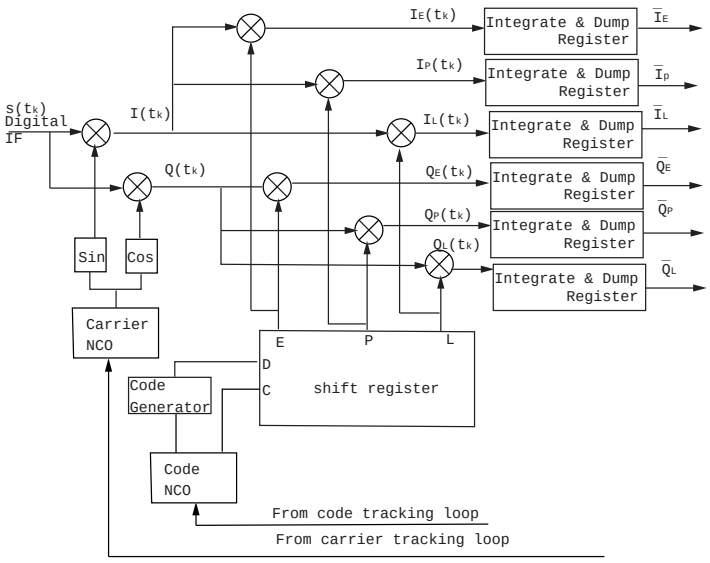

Figure 1: Code and phase wipeoff process

$$Q(t_k) = A\ C(t_k)\ D(t_k)\ \cos[\omega_{IF} t_k + \phi(t_k)] \sin[\omega_{IF} t_k + \hat{\phi}(t_k)] \tag{55}$$

The resulting in-phase and quadraphase baseband signal components are:

$$I(t_k) = \frac{1}{2} A\ C(t_k) D(t_k) \cos[\phi(t_k) - \hat{\phi}(t_k)] \tag{56}$$

$$Q(t_k) = \frac{1}{2} A\ C(t_k) D(t_k) \sin[\phi(t_k) - \hat{\phi}(t_k)] \tag{57}$$

The I and Q signals contain information about the difference between the incoming phase and estimated phase, but they are still modulated by the PRN code and data. The code generator generates early (E=$C(\hat{t}_k - \delta)$), prompt (P=$C(\hat{t}_k)$), and late (L=$C(\hat{t}_k + \delta)$) codes which are multiplied by $I(t_k)$ and $Q(t_k)$ to provide the six signals $I_E(t_k), I_P(t_k), I_L(t_k)$ and $Q_E(t_k), Q_P(t_k), Q_L(t_k)$, where δ is usually 1/2 code period. The code correlators average these three in-phase and three quadraphase components within a databit to provide $\bar{I}_E, \bar{I}_P, \bar{I}_L$ and $\bar{Q}_E, \bar{Q}_P, \bar{Q}_L$ for further processing. For example, the $\bar{I}_P$ and $\bar{Q}_P$ output by the accumulator can be expressed as:

$$\bar{I}_P = \frac{1}{2} A \sum_{k=1}^{n} D(t_k) C(t_k) C(\hat{t}_k) \cos[\phi(t_k) - \hat{\phi}(t_k)] \tag{58}$$

$$\bar{Q}_P = \frac{1}{2} A \sum_{k=1}^{n} D(t_k) C(t_k) C(\hat{t}_k) \sin[\phi(t_k) - \hat{\phi}(t_k)] \tag{59}$$

where n is the number of samples accumulated in the integration time T which is usually a C/A-code epoch period of one ms. When the estimated code and carrier phase match the incoming code and carrier phase, $C(t_k)C(\hat{t}_k) = 1$ and $\phi(t_k) - \hat{\phi}(t_k) = 0$. In this case $\bar{I}_p$ is the signal power while $\bar{Q}_p$ is noise.

The code and carrier NCO's are driven by signals from code and carrier tracking loops, see Fig 2. The channel filter is usually design by linearization of the code or phase detector resulting in a design model like that shown in Fig 3. Each channel of the traditional receivers works independently; therefore, they can not help each other in tracking. In addition, when a signal is blocked, the state of the filter and that channels NCO become corrupt. Signal reacquisition may require a two dimensional search to find the values for the delay $\Delta\tau$ and frequency f_D near the correct values and will require reconvergence of the state of the loop filter $F(s)$ and NCO. This is a serious deficiency in which the changing receiver antenna position and velocity are the dominant sources of error. The other receiver channels and the INS may have the position and velocity information available that can to eliminate this search and decrease the magnitude of the reconvergence transient.

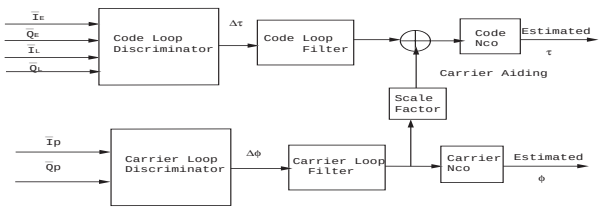

Figure 2: Conventional code and carrier tracking loops block diagram

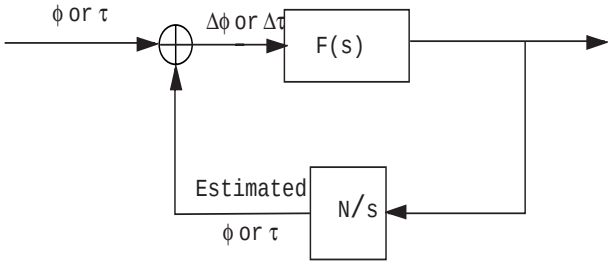

Figure 3: Conventional code or carrier tracking loop in math model

3.6.2 Proposed Approach

The proposed new aiding algorithm is illustrated in Fig 4. For the i-th active channel, the code phase error $\Delta\tau_i$ and carrier phase error $\Delta\phi_i$ are functions of in-phase and quadrature signals and they are expressed as follows:

$$\Delta\tau_i = g(\bar{I}_{E_i}, \bar{Q}_{E_i}, \bar{I}_{L_i}, \bar{Q}_{L_i}) \quad (60)$$

$$\Delta\phi_i = h(\bar{I}_{P_i}, \bar{Q}_{P_i}) \quad (61)$$

The receiver works with the conventional code and carrier tracking loops until it attains a stable navigation solution. Then it works with the new algorithm. For each channel, the proposed approach has a switch which allows selection of either the traditional loop filter or the INS to be used to drive the NCO's. When the signal strength is high, switch is set so that the traditional loop can be used and the channel's code and phase measurements are used to aid the INS. When the signal strength for a channel is low, then the INS drives the NCO. The INS is able to maintain tracking, because it is sensing the vehicle acceleration and angular rates and it is aided by the other channels that are still tracking. Once the satellite signal reappears, the receiver can resume tracking quickly. This is also true even if all the satellites are blocked out at the same time as long as the loss of all signals is not too long.

This approach was not able to be implement for a couple of reasons. The receiver processor is already running at maximum capacity. Therefore, the additional code required to run the above algorithms was not feasible on the receiver processor without rewriting the receiver software. It may have been possible to remove some aspects of the receiver software from that processor and implement a dual processor approach where the existing INS processor performed some of the required tasks. This would require significant interaction with Leica engineers, but is no longer possible as Leica has laid off its engineering division that was in Torrance CA. This is unfortunate for this project, as the proposed algorithm would significantly improve performance. Fortunately, other companies are progressing with INS aided GPS receiver designs.

3.7 Self-contained Prototype

The previous implementations of the UCR GPS/INS hardware used discrete components that were loosely distributed in the car. The GPS and base antennae were mounted on the car roof with the IMU, the GPS

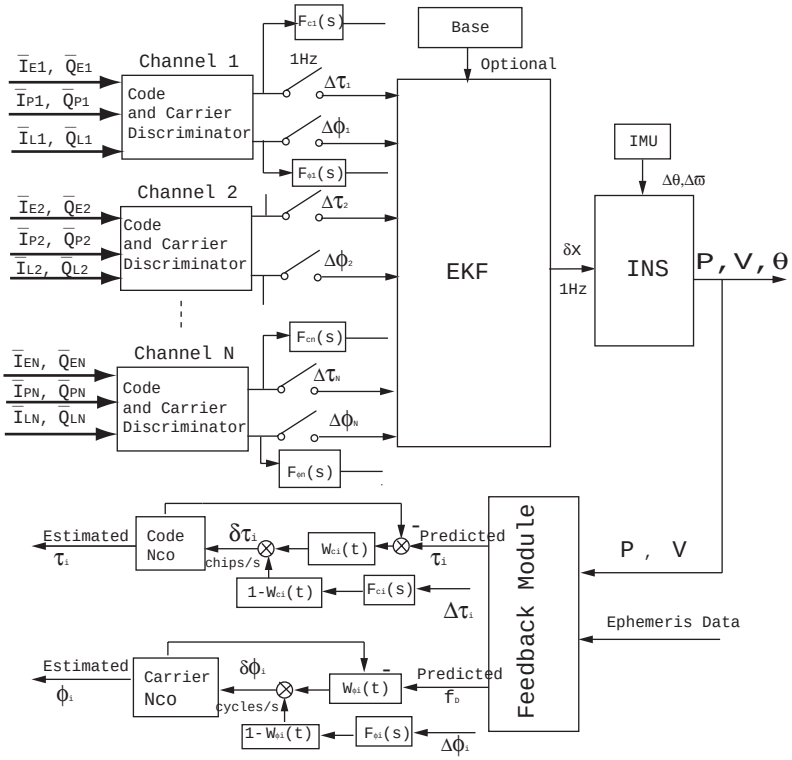

Figure 4: Proposed GPS/INS aiding algorithm

receiver was in the trunk, and the software was running on a notebook computer in the back seat of the car. An objective of this project was to organize the hardware into a more robust, self-contained unit that could be more easily mounted on test vehicles by non-specialists. This objective was accomplished, as described in this section.

The GPS aided INS navigation system consists of an embedded computer, two dual-frequency receivers (one is used as the Base and another as the Rover), two wireless modem OEM boards (i.e., base and rover), one IMU, one FIFO interface board between the parallel port and the receiver data bus, and, related accessories. The specifics of each item are listed in Table 1. Following are several photos related to the

	Model	Manufacture	Power
PC104	MSEBX-P3	Digital Logic	12v@15W
Receiver	ME500	Leica	12v@3.6W
Modem	FGR09CSU	Free Wave	12v@11W
IMU	YH-5000	YH Technology	12v@3W
FIFO Interface	**	UCR	**

Table 1: Hardware lists

new prototype implementation. Figure 5 is a signal flow block diagram. The PC104 has four serial ports and one parallel port. The radio modem is connected to serial port two, the IMU is connected to serial port three, and the control computer and magnetometer are connected to serial port four. The first serial port of the PC104 is currently free. The majority of these connections are internal to the prototype and would not be accessed by the typical user. Figure 6 is a photograph of the inside of the prototype. There is significant empty space and the hardware could fit into a smaller enclosure. For this stage of the project we made the decision to value ease of access over compactness. Figure 7 is a photograph of the outside of the prototype showing the external connections. The external connections are power (required), serial port to the control and magnetometer computer, ethernet, keyboard, mouse, and monitor. The keyboard, monitor, and mouse connections are optional and are used mainly for debugging and demonstration purposes. The ethernet connection is used for uploading and downloading software and data. Finally, there are two antenna

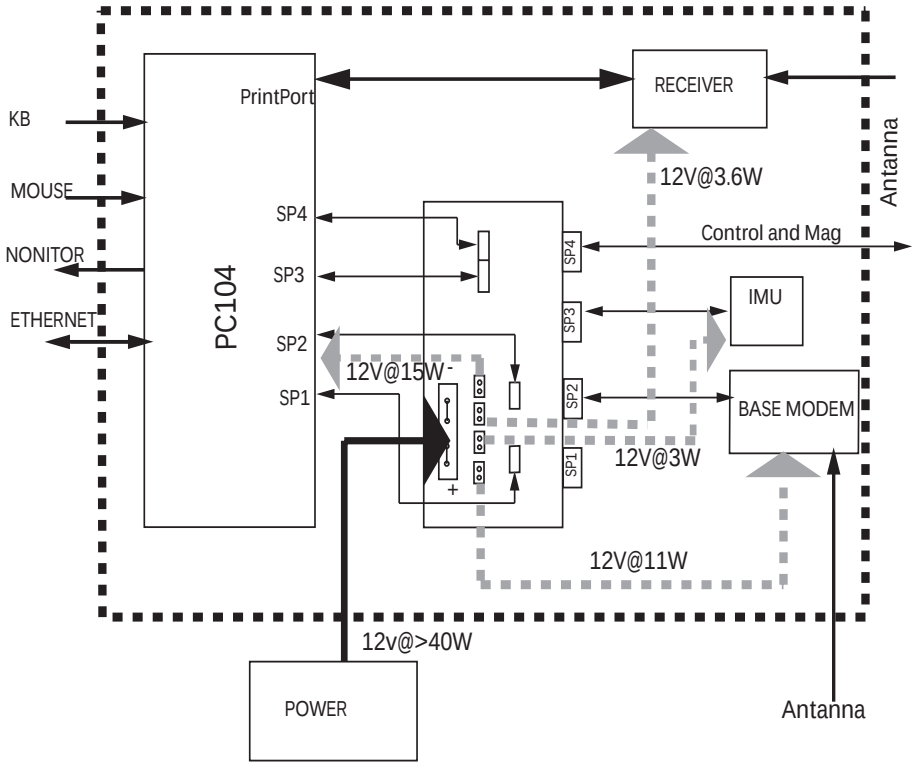

Figure 5: Connectivity of the GPS/INS Prototype Hardware.

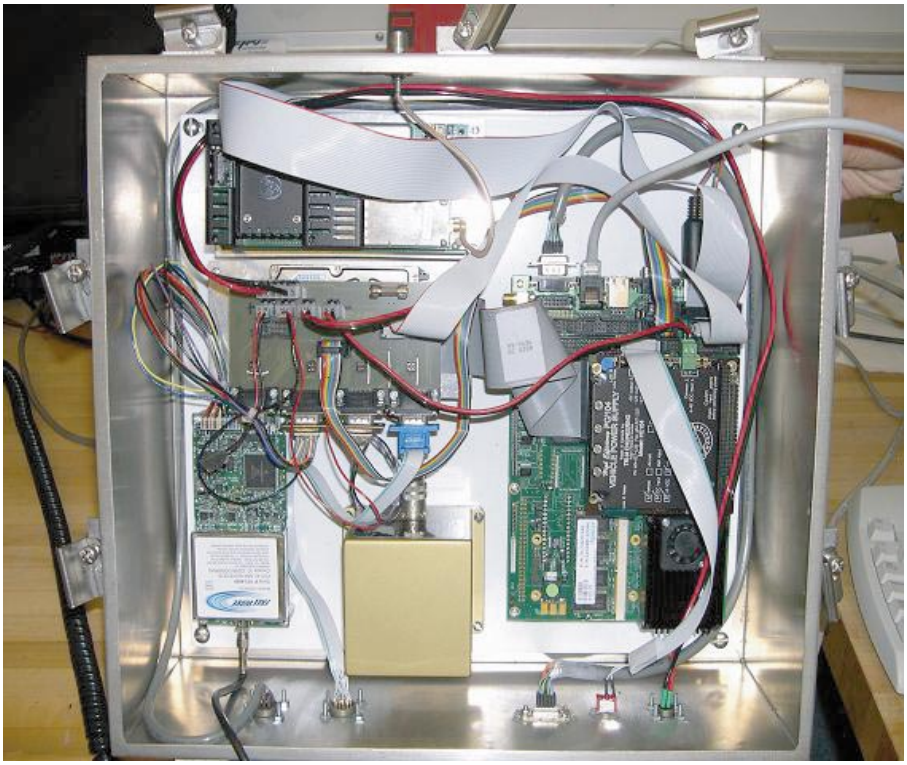

Figure 6: Photo of the inside of the GPS/INS prototype hardware box.

connections. One antenna is the two frequency GPS antenna. The other is the radio modem antenna. The Leica receiver board is an OEM board. The Leica receiver supports two versions of the receiver code, one version of the code outputs data via the serial port bus and one version outputs data via the parallel data bus. Corresponding to these two communication modes, UCR made two versions of a hardware interface board. To enable INS aiding of the GPS receiver, we choose to use the parallel port interface as it allows communication at greater than 1 MB/s. This required development if a parallel port interface circuit between the receiver and the PC104. The circuit schematic and pcb are shown in Figures 8-10.

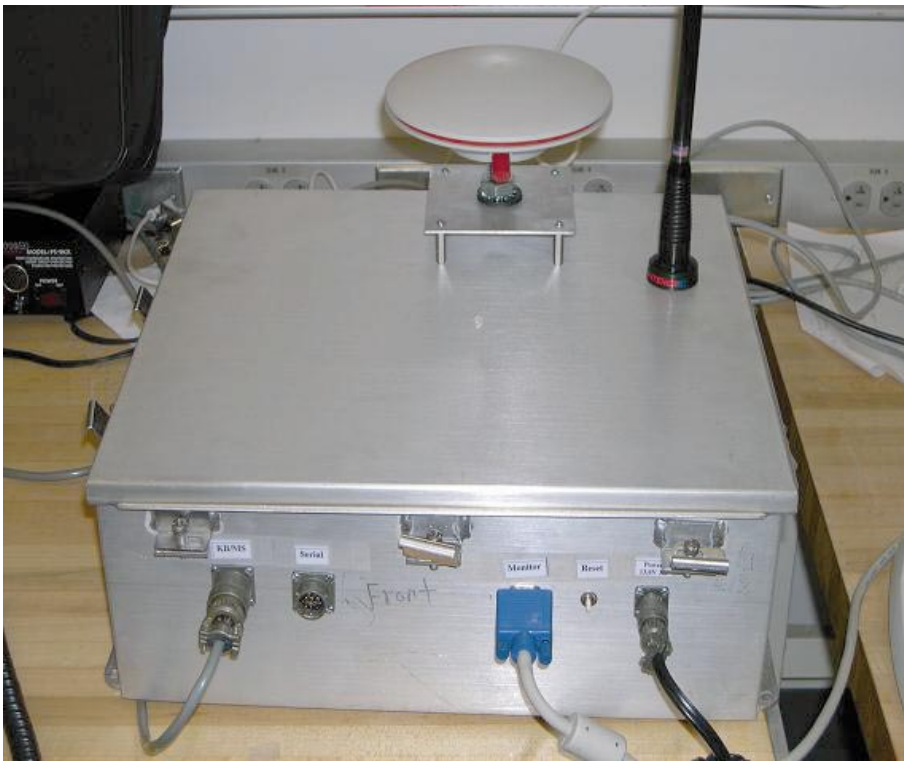

Figure 7: Photo of the outside of the GPS/INS prototype hardware box.

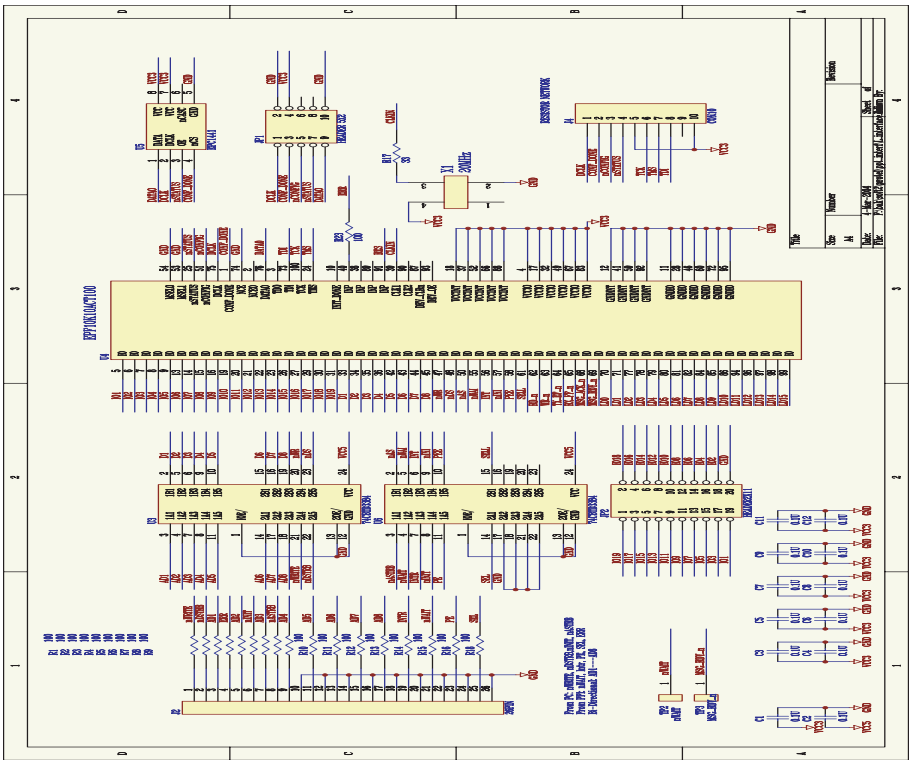

Figure 8: Portion one of the parallel port interface board schematic.

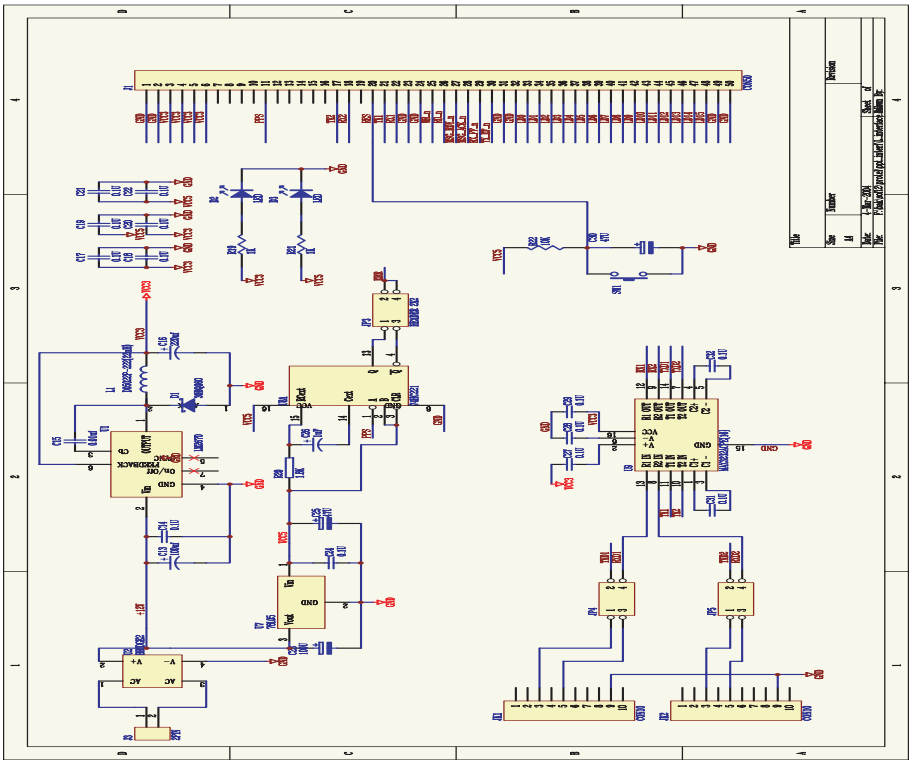

Figure 9: Portion two of the parallel port interface board schematic.

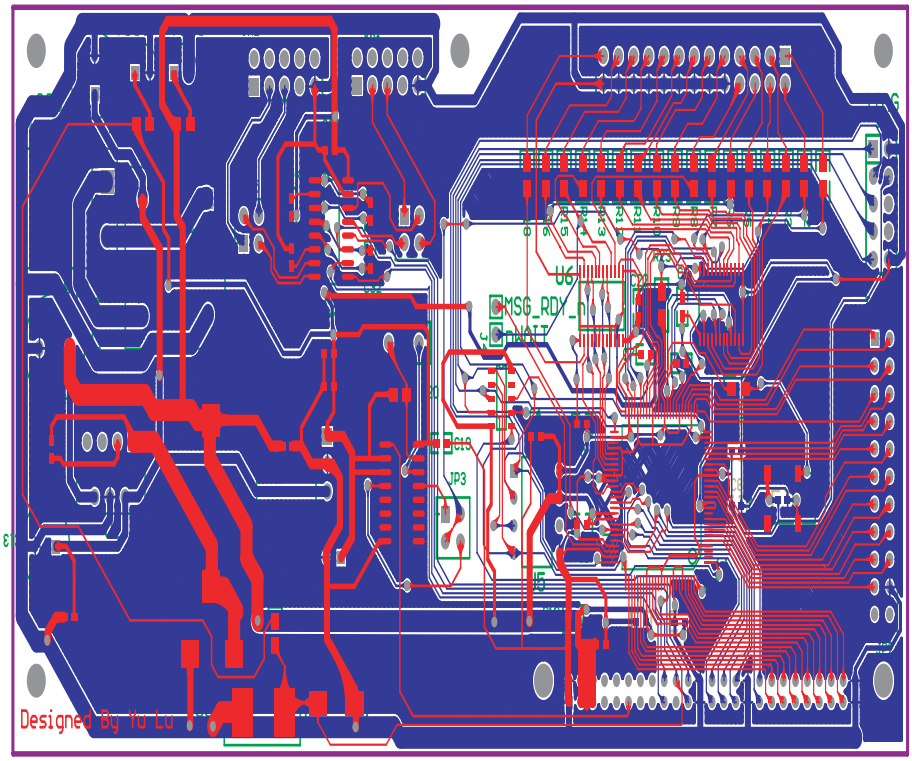

Figure 10: PCB board implementation of the parallel prot interface board.

4 Experimental Results

This section contains two sets of experimental results. First, we present the results of the aided integer ambiguity testing. Second, we present results from testing on a bus at Donners Pass.

4.1 Aided Integer Ambiguity: Test Results

The integer ambiguity resolution algorithm described in Section 3.5 was implemented and tested in two separate tests.

In the lab we have two receivers connected to two separated antenna which are 6 meters apart. One is used as a base station. One is used as the rover. The algorithm described in Section 3.5 will typically solve the integer ambiguities instantaneously and correctly without altitude aiding if there are six or more satellites are available. Therefore, to evaluate the utility of altitude aiding the test is carried out in situations where only five satellites are available. During the test, is repeated every second. This involves: searching for the integers; storing the number of correctly locked satellites; and, reinitializing the integer search process for the next second of data. The thresholds for validating the integers on a per satellite basis are as followings: $|res_{12}| < 0.027m$, $|res_{1n}| < 0.012m$, $|res_{1w}| < 0.095m$.

The experimental results (based on 11999 epochs) show that, while the GPS-only integer resolution process successfully found and declared the correct integers with 5 satellites for 18% of the trials. The altitude aided GPS resolved the integer successfully at a 98% rate. Using altitude aiding and the decision thresholds of the previous paragraph, the correct integers were accepted at an 87% rate and incorrect integers were never accepted.

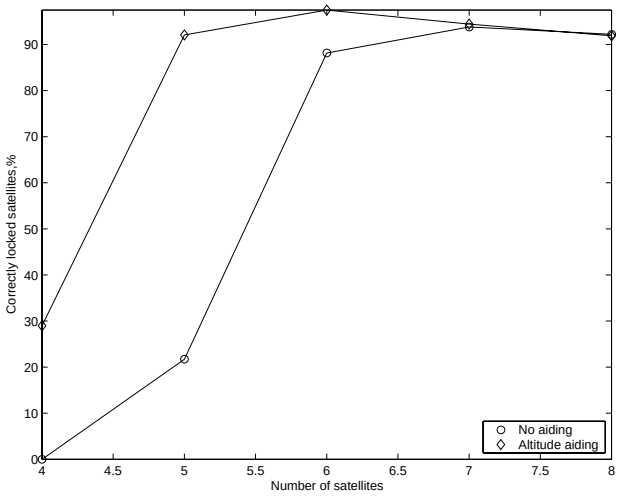

Figure 11: Percentage of epochs in which all n integers are correctly resolved, where n is the number of available satellites. The experiment involved 4415 epochs and a 2.8-kilometer baseline

A second experiment was carried out with a longer baseline of 2760 m to further evaluate the aiding algorithm in a more realistic situation. As illustrated in Figure (11), the performance with altitude aiding is much better than without aiding when there are less than seven satellites in view. For example, with only five satellites, the altitude aided algorithm finds the correct integers with a 92.02% sucess rate while the none-aided integer resolution only succeeds at a 21.70% rate. This experiment is based on 4415 epochs.

4.2 Donners Pass Testing

In November 2003, UCR personnel visited PATH and Donners Pass. The goal was to have an extensive debugging and testing session with PATH personnel, followed by control demonstrations on a bus. The control demonstrations included the magnetometer and GPS aided INS running on the bus and being used as the inputs to the control system. Various experiments were run:

- magnetometer and GPS aided INS controlling the vehicle;
- magnetometer and GPS aided INS controlling the vehicle while the drive added disturbances by yanking on the steering wheel;
- the driver switching back and forth between magnetometer and GPS aided INS controlling the vehicle and magnetometer only controlling the vehicle;
- magnetometer and GPS aided INS controlling the vehicle while it performed lane relative maneuvers.

For all of Figures 12–25 the top graph shows the distance from the trajectory versus time. For all figures except Figures 24 and 25 the red curve is the magnetometer measurement of distance and the blue curve is the INS estimate of the distance. In Figures 24 and 25, the red curve is the off trajectory distance during a 3.6 m lane change and the blue curve is the error relative to the lane change maneuver. The second plot from the top is the velocity of the vehicle normal to the trajectory. The third plot is the trajectory relative heading error. The fourth plot is the vehicle yaw rate from the INS (blue) and from the PATH gyro (red). The fifth plot is the control flag. The INS control state is driving the lateral controller when this flag has the value of 1.0. The magnetometer control state is driving the lateral controller when this flag is set to 0.0. In spite of the value of this flag, if the distance and heading error plots become flat (e.g., see t = 100–125 in Figure 19), then the driver is manually steering the vehicle. The bottom plot shows the steering wheel angle as commanded by the lateral controller. If it becomes flat, that the driver is controlling the vehicle manually.

Throughout these runs, the driver is able to and does grab the steering wheel and turn it. This cause the vehicle to depart slightly from the trajectory so that we can observe control convergence transients.

These runs were very satisfying. First, the INS control state and magnetometer control state matched very well. This is true both when only the DCPGPS is aiding the INS and when both the magnetometer and DCPGPS are aiding the INS. Second, we were able to demonstrate seamless transitions between magnetometer control, INS control, and manual control. These switches were made in many different orders and scenarios with very good performance. Third, we were able to demonstrate advanced maneuvers such as lane changes.

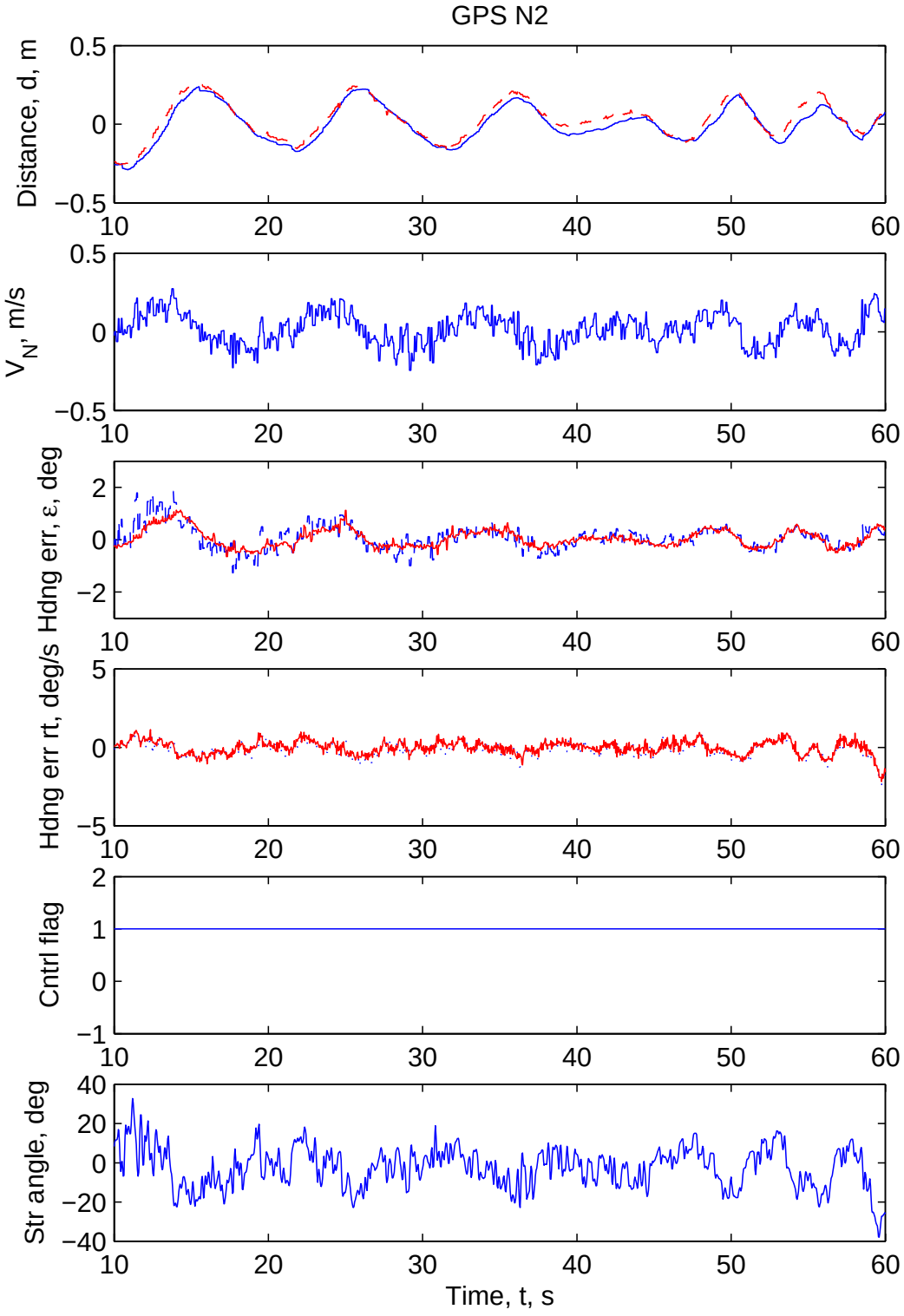

Figure 12: This run uses only DCPGPS to aid the INS. Note that the control flag is 1.0 for the entire run, which indicates that the INS state is used as input to the control law for the entire run. This is a northbound run. During this run, the minimum, average, maximum vehicle speeds were 6.0, 14.8, and 19.5 m/s

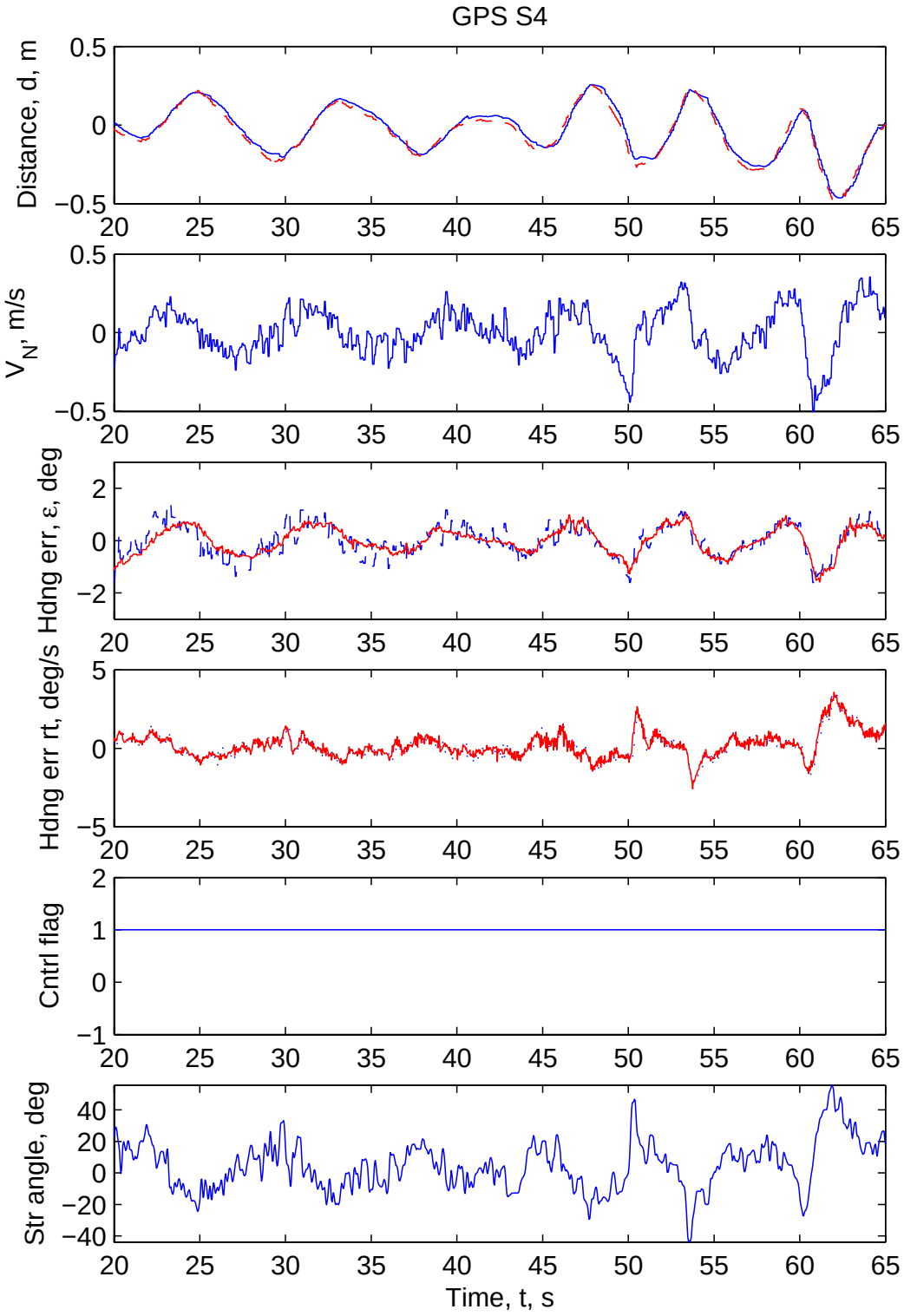

Figure 13: This run uses only DCPGPS to aid the INS. The INS state is used as input to the control law for the entire run, but the driver is occasionally perturbing the vehicle from the trajectory by grabbing and deflecting the steering wheel. This is a southbound run. During this run, the minimum, average, maximum vehicle speeds were 7.9, 13.7, and 18.7 m/s

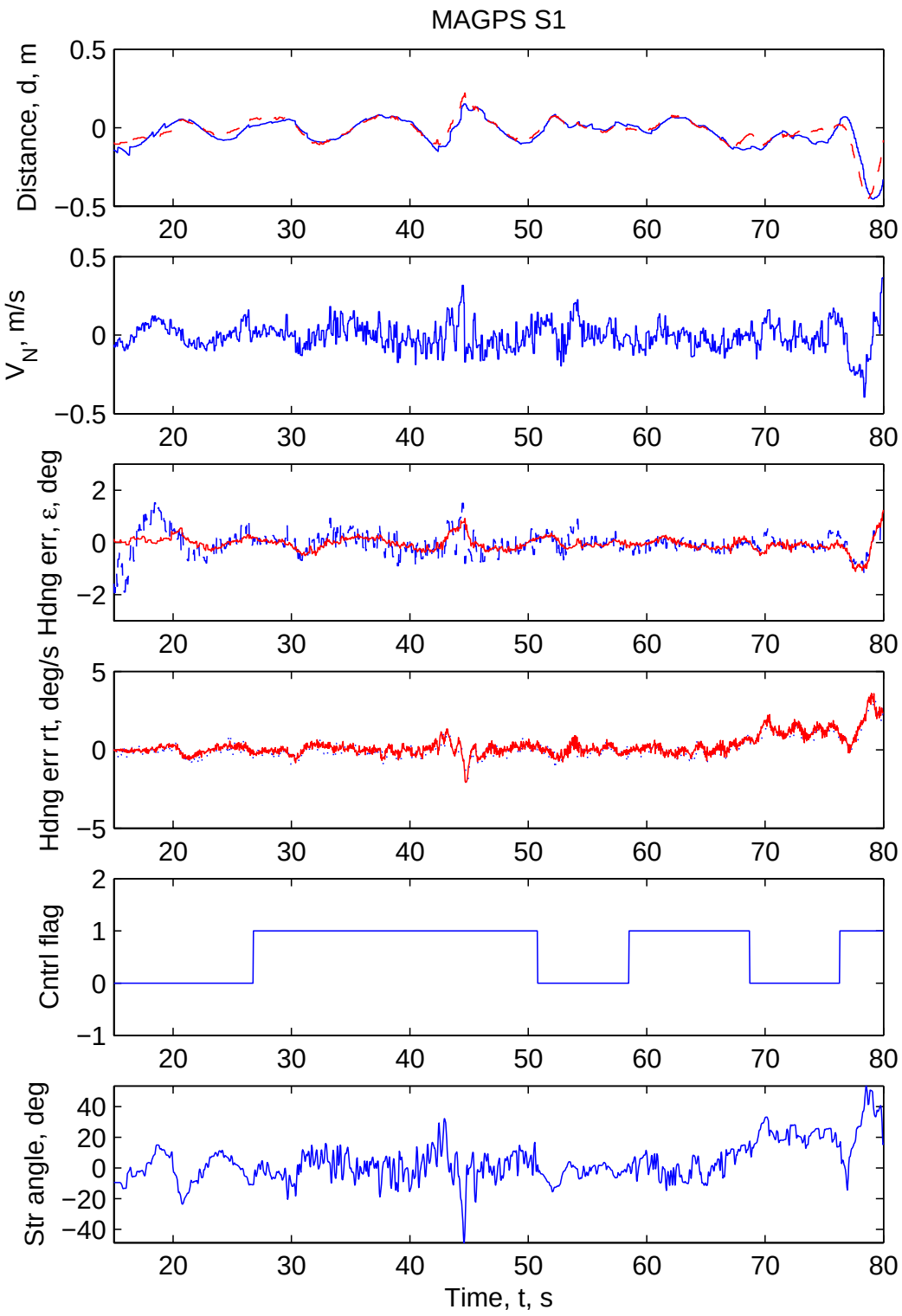

Figure 14: This run uses only GPS aiding of the INS. The input to the control law is switched back and forth by the driver between the magnetometer control state and the DCPGPS-aided-INS control state. Control flag equal to 1 indicates that the INS state is input to the controller, while the control flag equal to 0 indicates that the magnetometer state is input to the controller. Note that the controller switches between the two control states very smoothly. No tracking error transients are observed following the switches. At approximately 45 s, the driver perturbs the vehicle by grabbing the steering wheel. At t=75 s, the vehicle is entering the curved portion of the trajectory. This is a southbound run. During this run, the minimum, average, maximum vehicle speeds were 2.2, 12.5, and 18.5 m/s

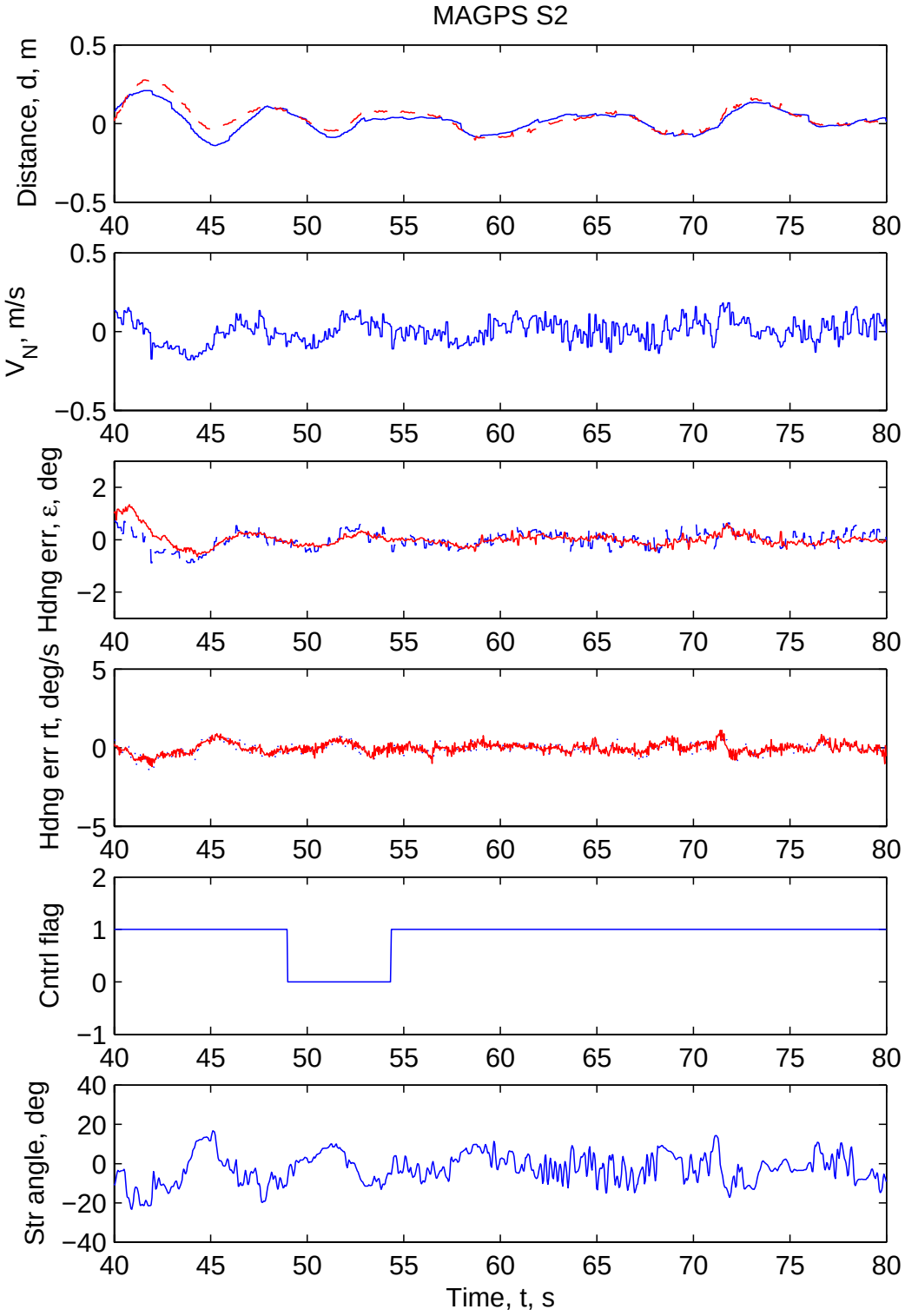

Figure 15: This run uses only DCPGPS aiding of the INS. The input to the control law is switched back and forth by the driver between the magnetometer only and the DCPGPS-aided-INS control states. Control flag equal to 1 indicates that the INS state is input to the controller, while the control flag equal to 0 indicates that the magnetometer state is input to the controller. Note that the controller switches between the two control states very smoothly. This is a southbound run. During this run, the minimum, average, maximum vehicle speeds were 10.7, 14.4, and 16.6 m/s

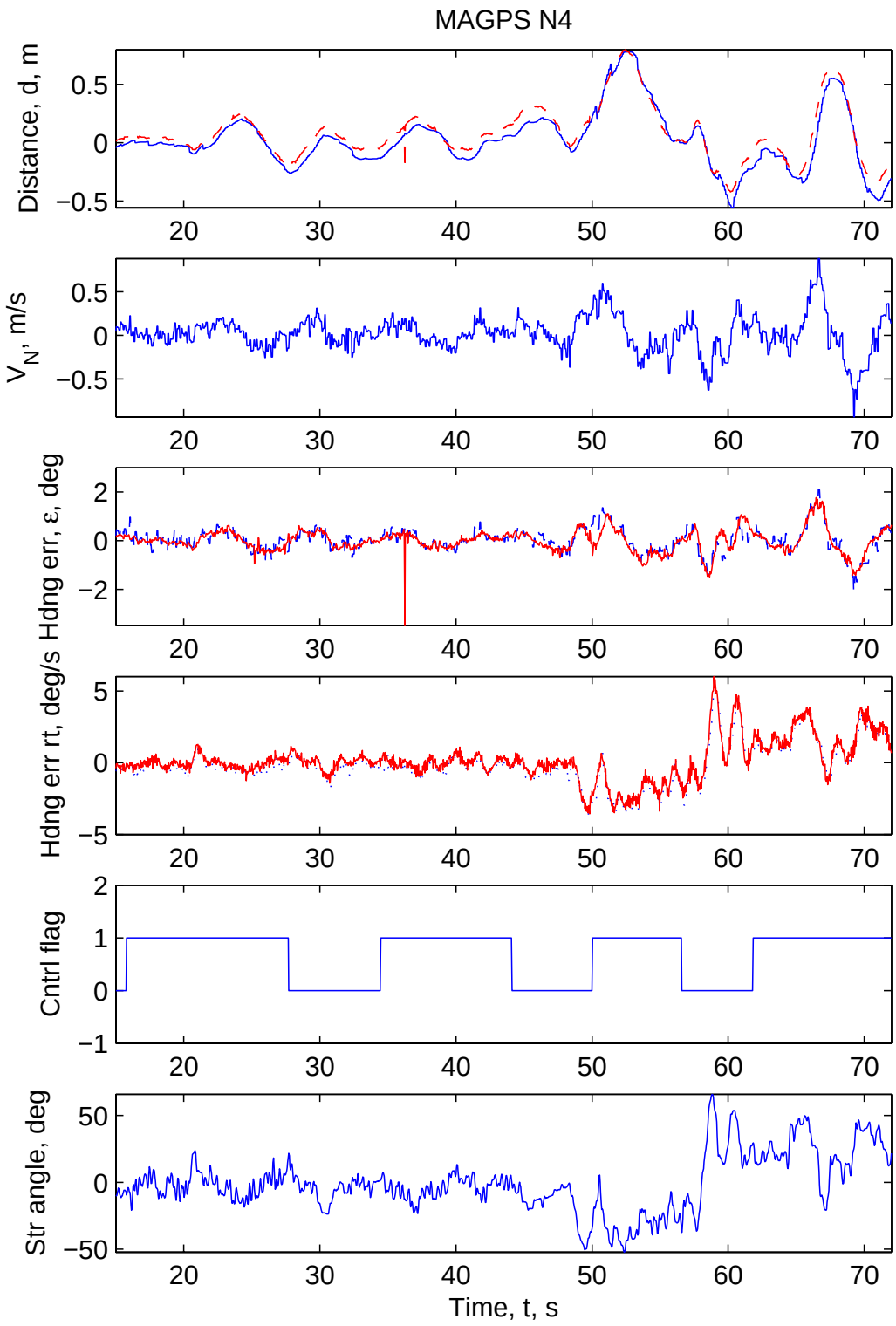

Figure 16: This run uses only DCPGPS aiding of the INS. The input to the control law is switched back and forth by the driver between the magnetometer control state and the INS control state. Control flag equal to 1 indicates that the INS state is input to the controller, while the control flag equal to 0 indicates that the magnetometer state is input to the controller. Note that the controller switches between the two control states very smoothly. Not transients are observed. At approximately t=48 and t=58, the vehicle is entering the sections of the trajectory where the curvature switches. The spikes in the magnetometer measurements near t-37 s are locations where two magnet trajectories intersect. This is a northbound run. During this run, the minimum, average, maximum vehicle speeds were 12.5, 21.8, and 25.3 m/s

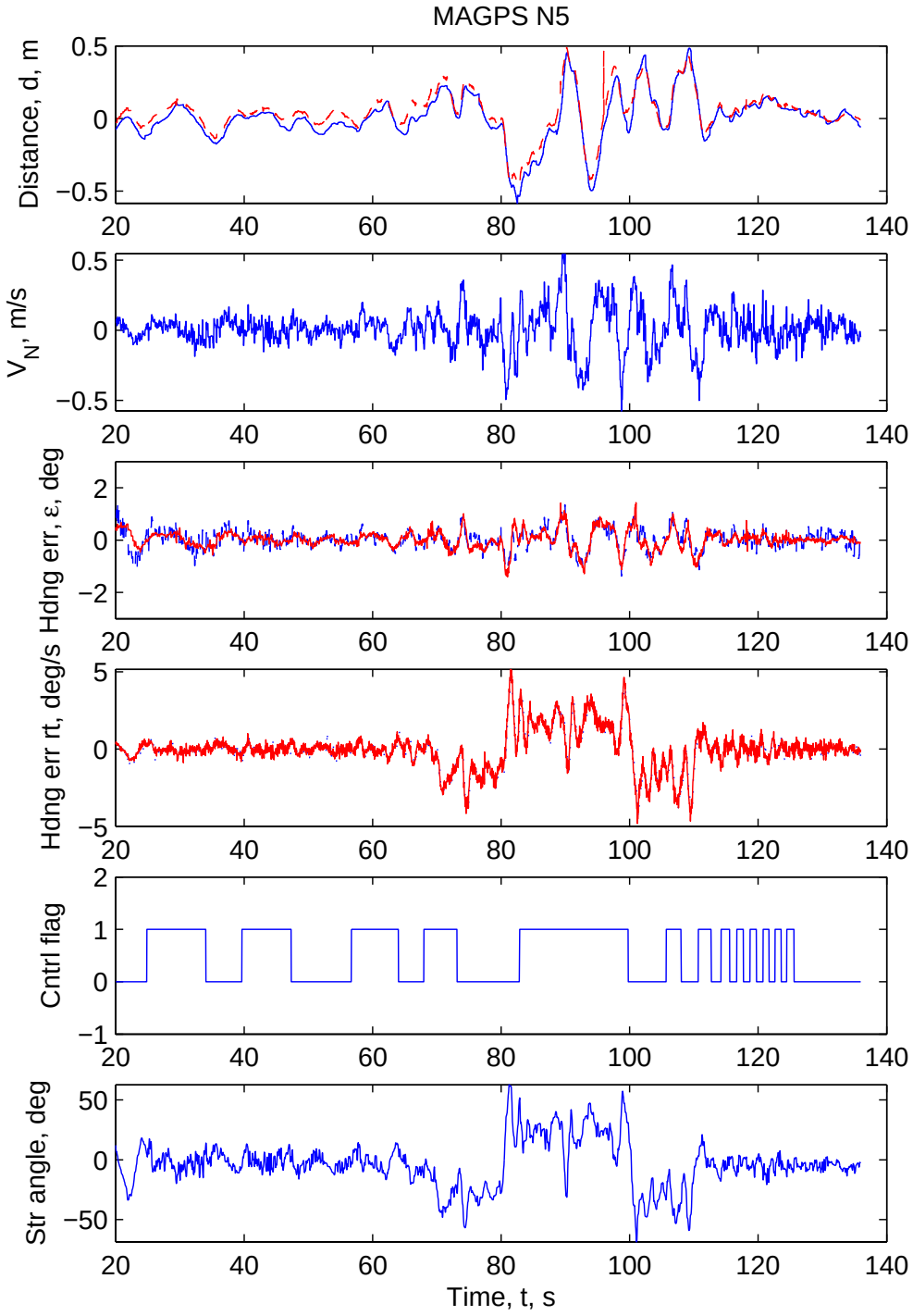

Figure 17: This run uses only DCPGPS aiding of the INS. The input to the control law is switched back and forth by the driver between the magnetometer control state and the INS control state. Control flag equal to 1 indicates that the INS state is input to the controller, while the control flag equal to 0 indicates that the magnetometer state is input to the controller. Note that as indicated by the control flag, the switching between the two controllers is frequent near the end of the run. Still, control is accurate and no switching transients are observed. The three sections where the trajectory has step changes in curvature are clearly observable between t = 70 and t=110 s. At approximately t=90s, the driver perturbs the vehicle by grabbing the steering wheel. This is a northbound run. During this run, the minimum, average, maximum vehicle speeds were 3.8, 19.3, and 26.0 m/s

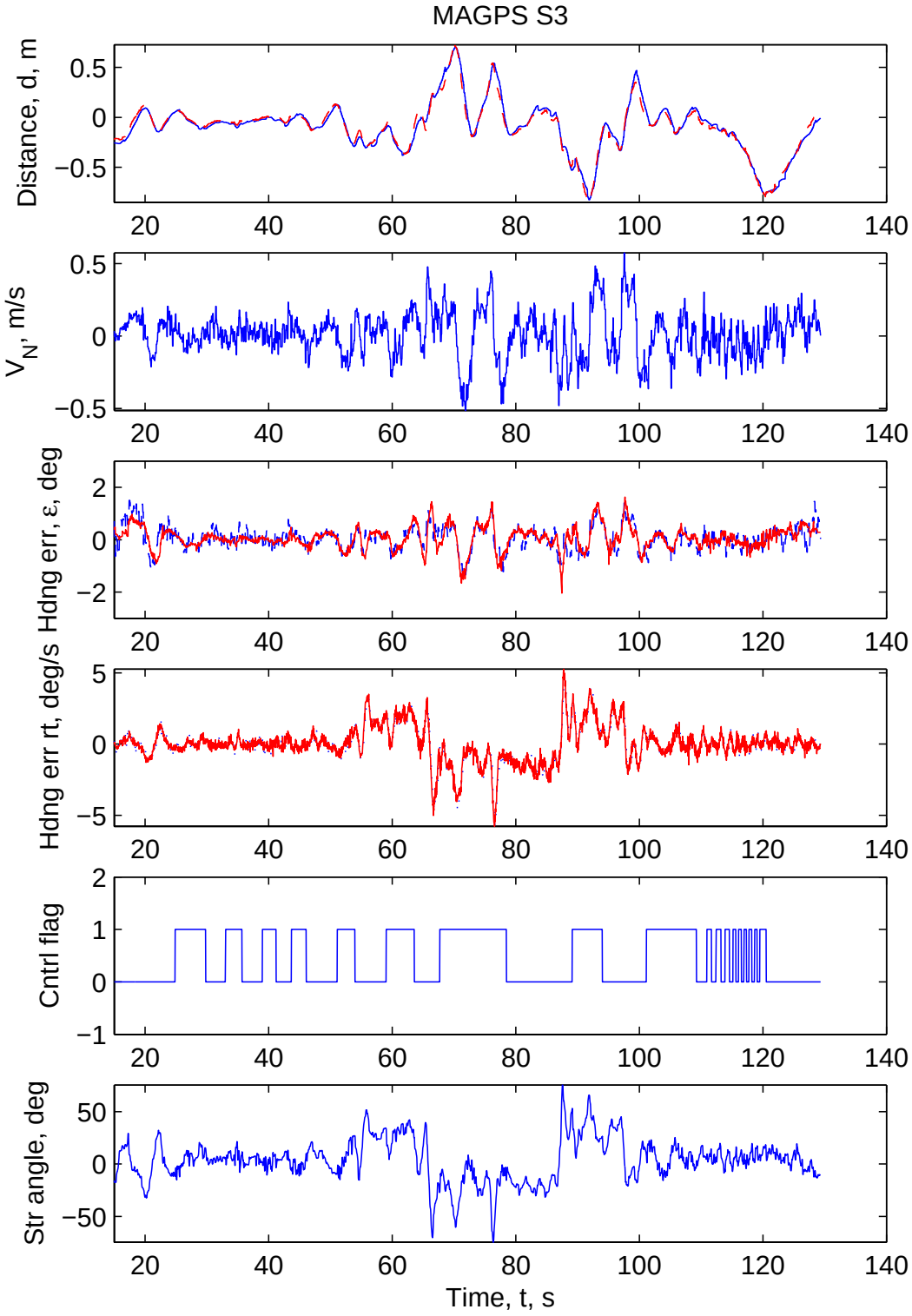

Figure 18: This run uses both magnetometer and DCPGPS aiding of the INS. The input to the control law is switched back and forth between the magnetometer control state and the INS control state, as indicated by the control flag. Near the end of the run, the switching is frequent. No transients are observed, but the vehicle does slowly depart from the trajectory due to the switching. This is a southbound run. The curved portion of the trajectory (three step changes in curvature) is easily observed between t=50 and t=100 s. During this run, the minimum, average, maximum vehicle speeds were 2.9, 19.7, and 26.3 m/s

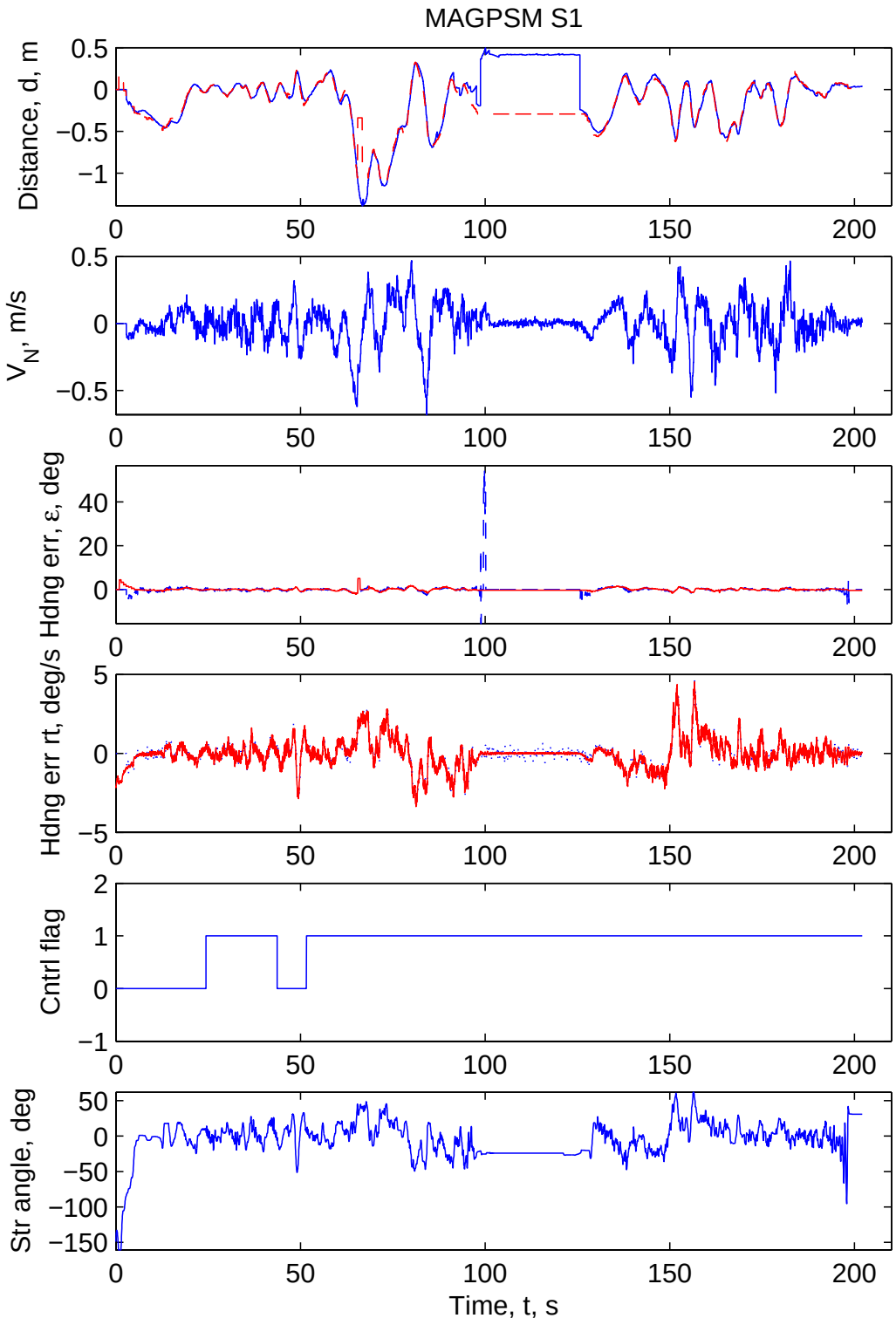

Figure 19: This run uses both magnetometer and DCPGPS aiding of the INS. The input to the control law is switched back and forth by the driver between manual driving, the magnetometer control state and the INS control state. Manual driving occurs between t=100 and t=130s. At the end of this time, automatic control using the INS state is turned back on with a smooth transition. This is a southbound run. During this run, the minimum, average, maximum vehicle speeds were 0.0, 10.9, and 24.5 m/s

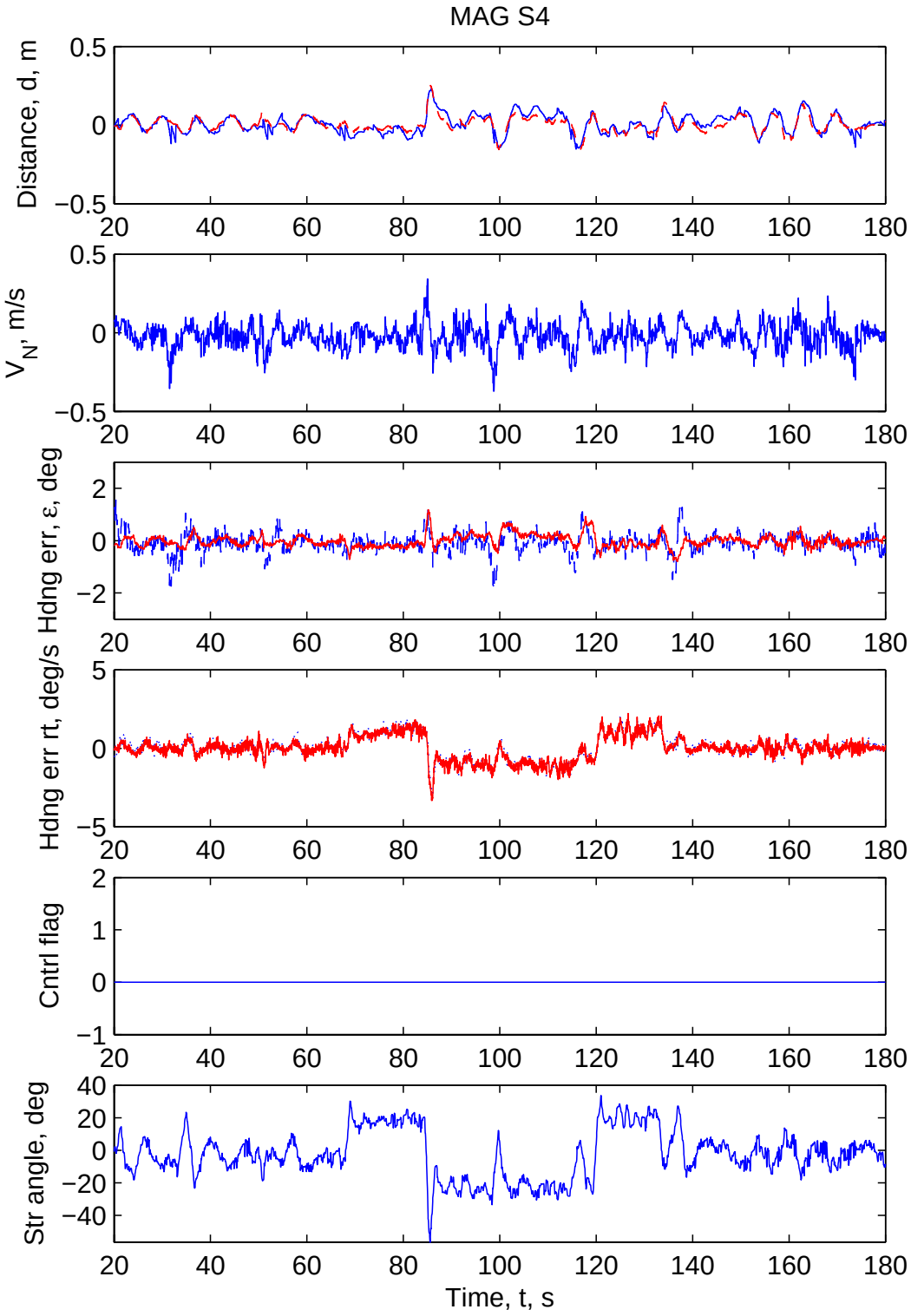

Figure 20: This run uses both magnetometer and DCPGPS aiding of the INS. The input to the control law is always the magnetometer only control state. This is a southbound run. The portions of the trajectory where the step changes in curvature occur are clearly visible between t=70 and t=140 s. During this run, the minimum, average, maximum vehicle speeds were 3.4, 13.4, and 23.2 m/s

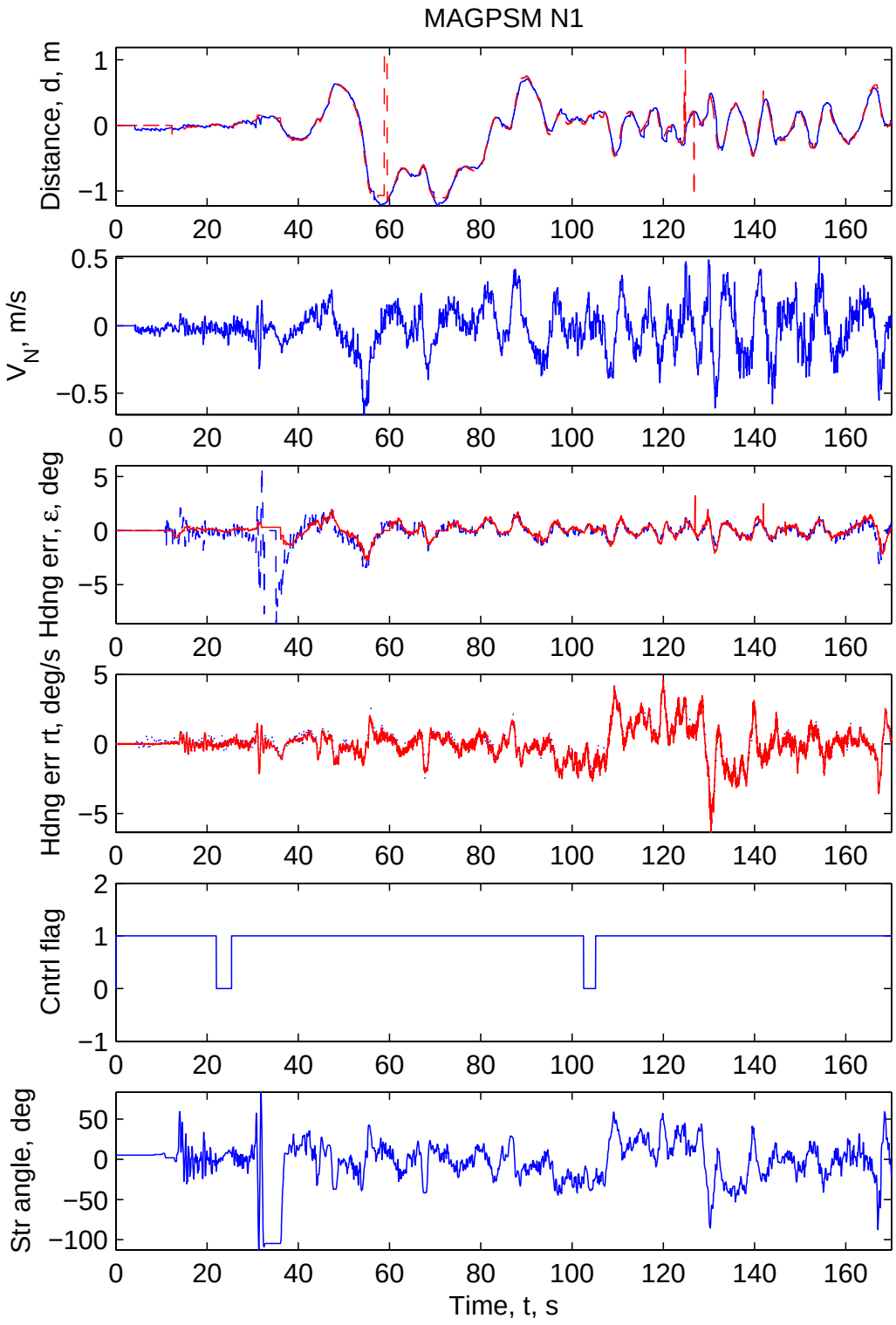

Figure 21: This run uses both magnetometer and DCPGPS aiding of the INS. The input to the control law is switched back and forth by the driver between the magnetometer control state and the INS control state. The spikes in the magnetometer data are locations along the trajectory where two magnet trajectories intersect. This is a northbound run. During this run, the minimum, average, maximum vehicle speeds were 0.0, 13.4, and 27.5 m/s

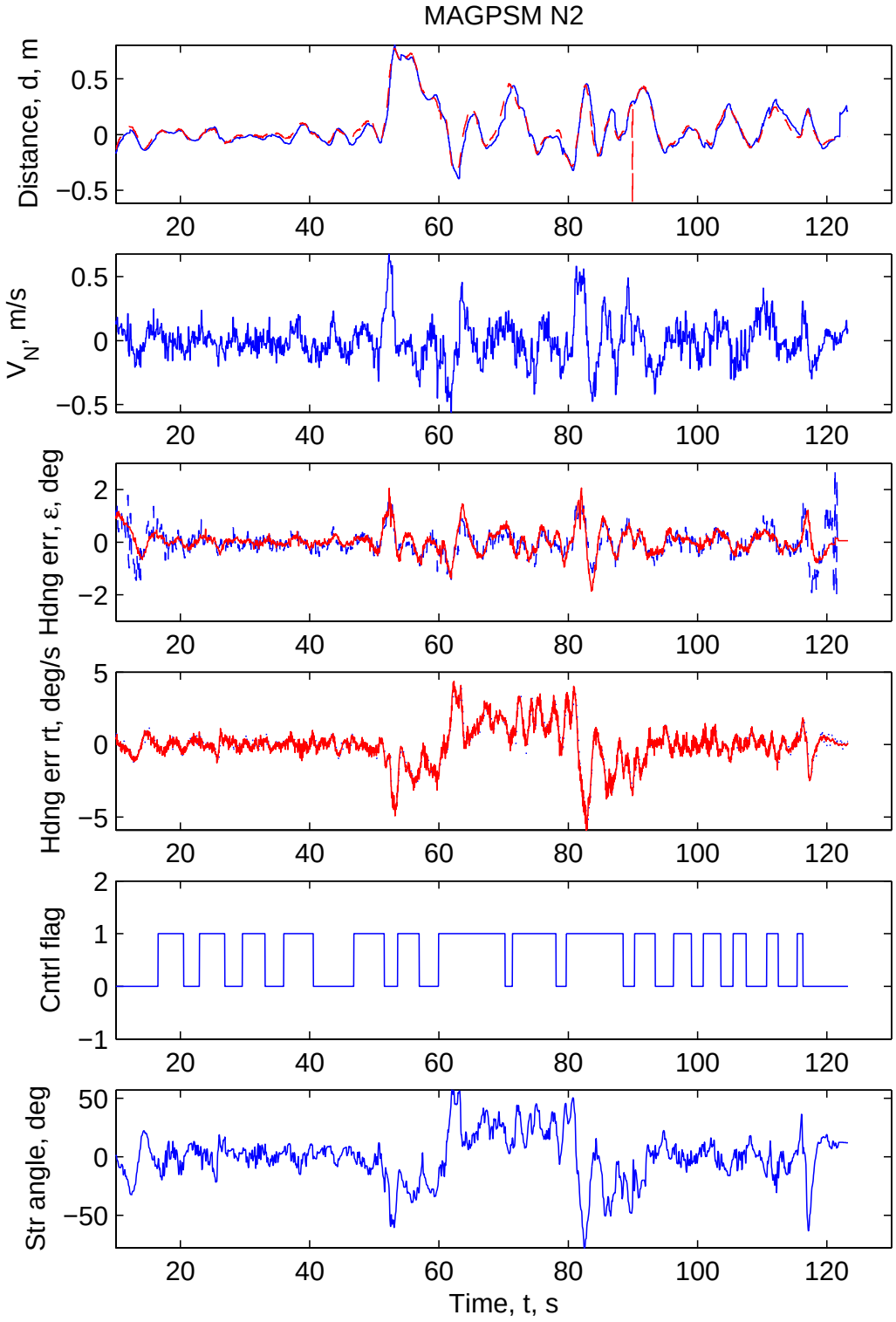

Figure 22: This run uses both magnetometer and DCPGPS aiding of the INS. The input to the control law is frequently switched back and forth by the driver between the magnetometer control state and the INS control state. The spike in the magnetometer data are locations along the trajectory where two magnet trajectories intersect. This is a northbound run. The three step changes in curvature are observed between t=50 and t=95 s. During this run, the minimum, average, maximum vehicle speeds were 0.0, 19.8, and 25.6 m/s

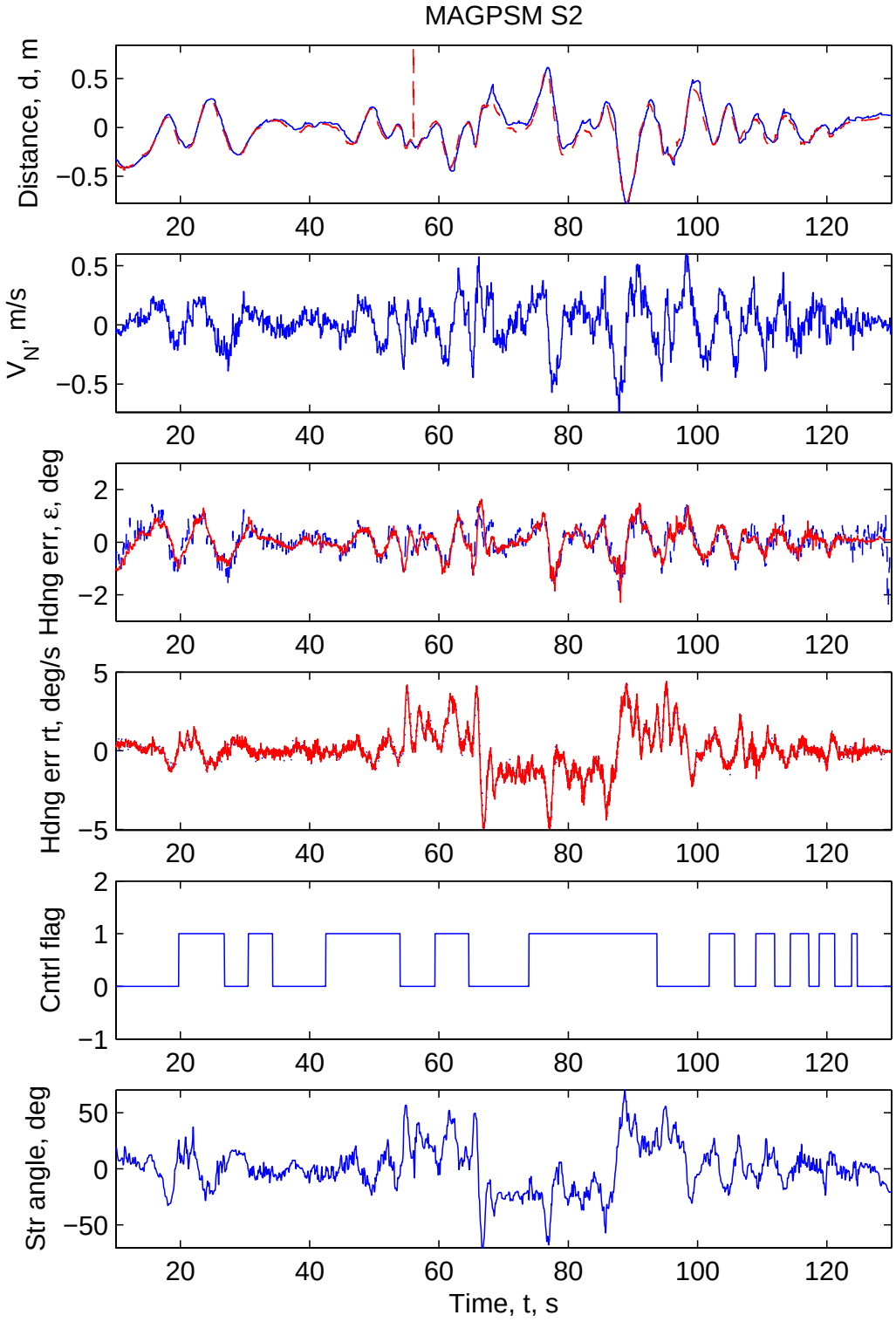

Figure 23: This run uses both magnetometer and DCPGPS aiding of the INS. The input to the control law is switched back and forth by the driver between the magnetometer control state and the INS control state. The spikes in the magnetometer data are locations along the trajectory where two magnet trajectories intersect. This is a southbound run. The three step changes in curvature are observed clearly in the plots of yaw rate and steering angle between t=50 and t=100 s. During this run, the minimum, average, maximum vehicle speeds were 0.0, 18.3, and 25.2 m/s

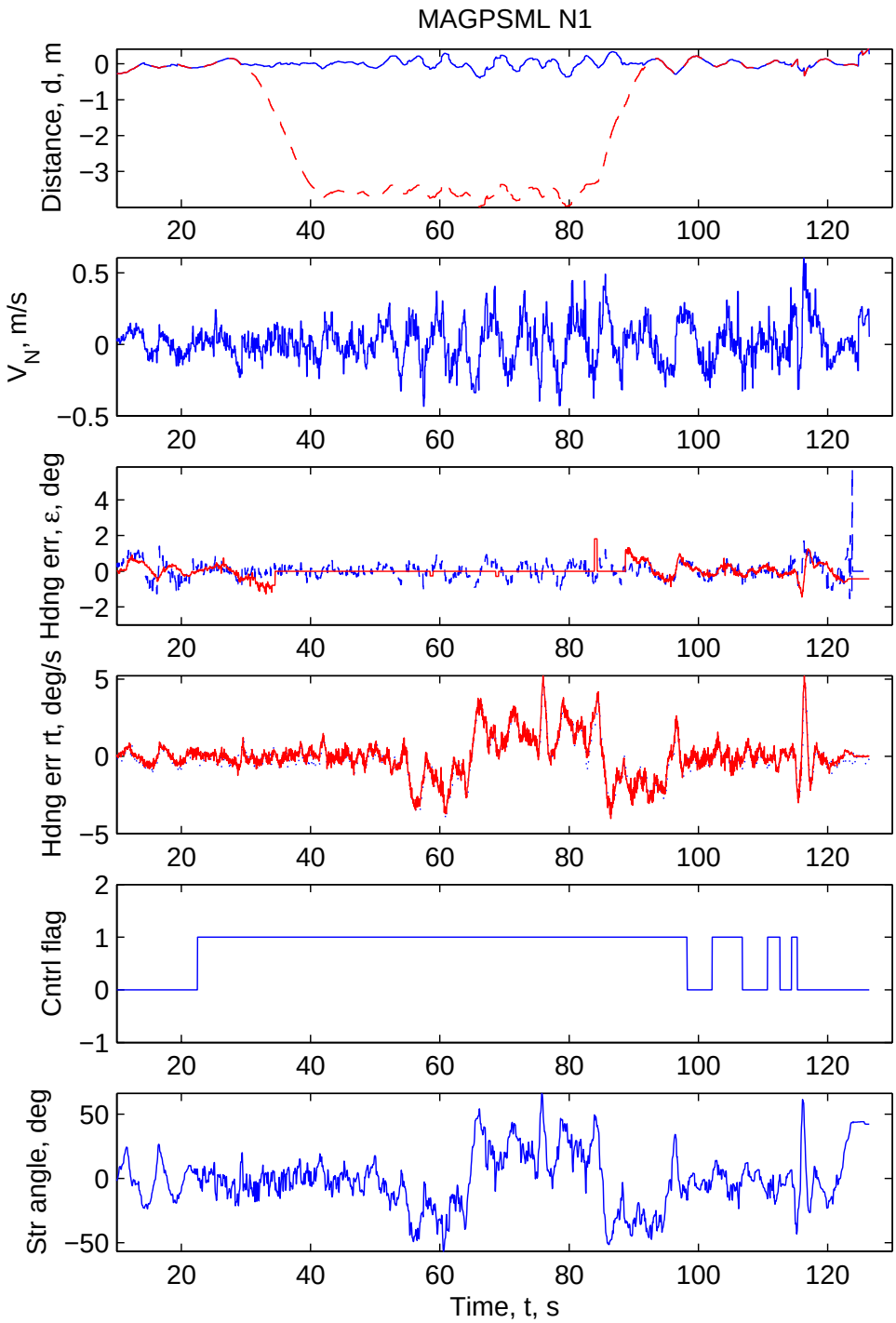

Figure 24: This run uses both magnetometer and DCPGPS aiding of the INS. During this run the vehicle is commanded to perform a 3.6m lane change. The input to the control law is switched back and forth by the driver between the magnetometer control state and the INS control state. During the maneuver, only the INS control state is used, as the maneuver is to far from the magnets in the roadway for the magnetometer measurement to be available. In the top graph, the red curve is the INS estimate of distance from the lane centerline defined by the trail of magnets. The blue curve is the tracking error relative to the defined maneuver. Note that when the vehicle is more than 0.9 m from the strip of magnets, the magnetometer heading error curve (red in plot three) is zero, since the magnetometer is not taking measurements. Note also that the lane change maneuver is performed through the curved portion of the trajectory. This is a northbound run. During this run, the minimum, average, maximum vehicle speeds were 0.0, 19.3, and 26.7 m/s

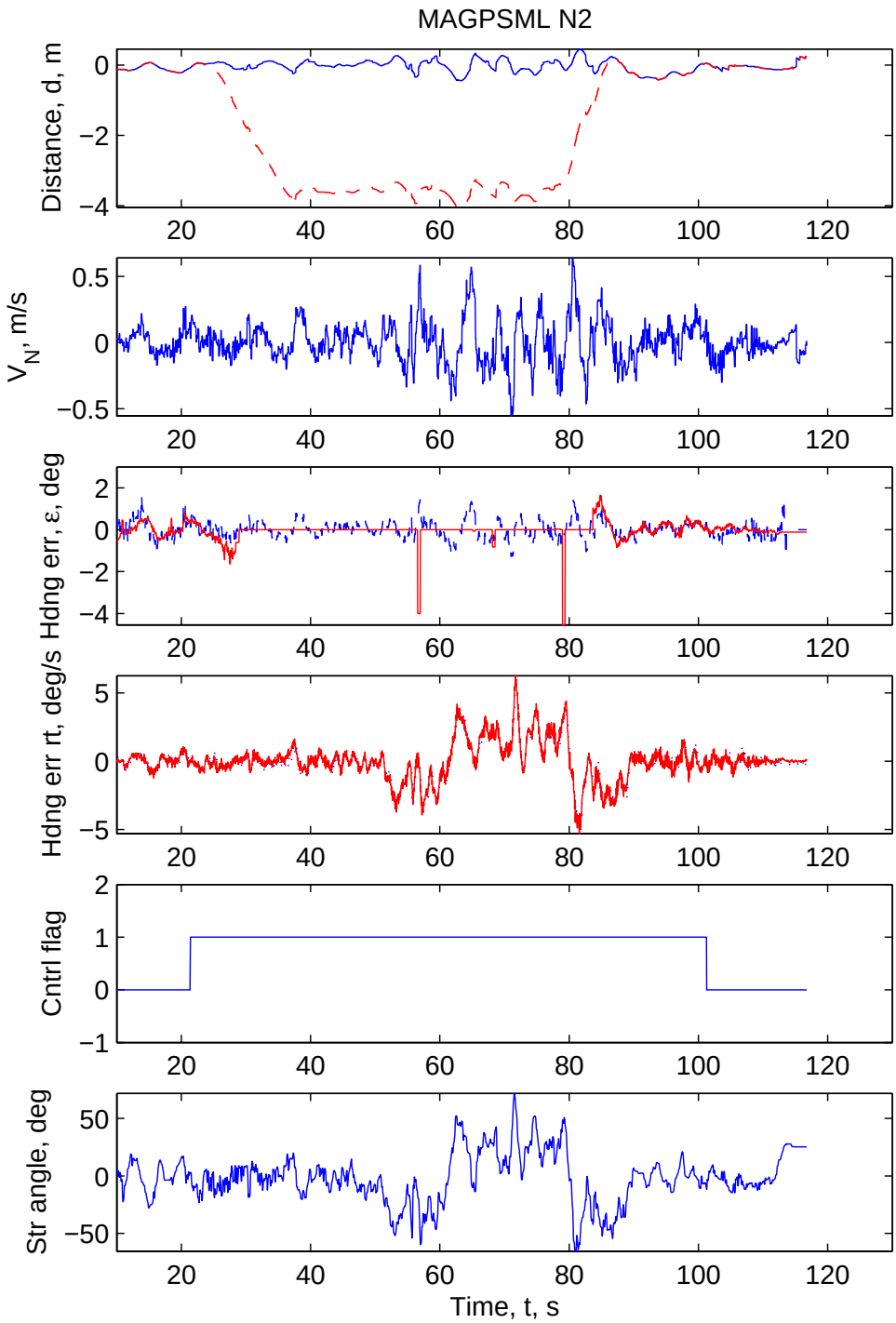

Figure 25: This run uses both magnetometer and DCPGPS aiding of the INS. During this run the vehicle is commanded to perform a 3.6m lane change. The input to the control law is switched back and forth by the driver between the magnetometer control state and the INS control state. During the maneuver, only the INS control state is used, because the maneuver takes the vehicle beyond the range of the magnetometer. In the top graph, the red curve is the INS estimate of distance from the lane centerline defined by the trail of magnets. The blue curve is the tracking error relative to the defined maneuver. Note that when the vehicle is more than 0.9 m from the strip of magnets, the magnetometer heading error curve (red in plot three) is zero, since the magnetometer is not taking measurements. The two spikes in the magnetometer heading are due to crossing of other magnet trajectories. Note also that the lane change maneuver is performed through the curved portion of the trajectory. This is a northbound run. During this run, the minimum, average, maximum vehicle speeds were 0.0, 19.8, and 27.9 m/s

5 Conclusions

This project has been very interesting and successful. In preparing for participation in Demo2002, we constructed much more robust prototypes of our DCPGPS aided INS hardware. This include significant software re-writing that improved the reliability of the software. Overall, the hardware and software are now much more reliable and easier to use and install on test vehicles. A new algorithm was designed , but not implemented, for INS aiding of a GPS receiver. We expect that this approach would lead to better satellite tracking during brief interruptions of the satellite signal. Implementation would require extensive interactions with the receiver design team, which is no longer possible due to changes in the GPS industry. We have developed new algorithms to use information from non-GPS sensors to facilitate and speed up the process of integer ambiguity resolution. This algorithm was evaluated in two experiments at UCR with significant improvements in the ability to correctly identify the integer ambiguities in a single epoch with fewer than 6 satellites. This algorithm was also used during the Crows Landing testing. Finally, UCR and PATH worked at PATH and Crows Landing and generated an impressive set of data as shown in Figures 12–25 of Section 4.2. This set of experiments was the culmination of the project. The experiments mounted the GPS/INS hardware on a bus that already was instrumented with the magnetometer hardware. We demonstrated that (1) the INS control state and magnetometer control state matched very well both when only the DCPGPS is aiding the INS and when both the magnetometer and DCPGPS are aiding the INS; (2) seamless transitions between magnetometer control, INS control, and manual control; (3) advanced maneuvers such as lane changes.

6 Publications Resulting from this Project

To date, this project has generated the following publications:

1. J. A. Farrell, Han-Shue Tan, Yunchun Yang, Carrier Phase GPS-aided INS based Vehicle Lateral Control. ASME Journal of Dynamics Systems, Measurement, & Control. 42 M.S. pages. Accepted September 2002.

2. H.-S. Tan, B. Bougler, J. A. Farrell, and Y. Yang, Automated Steering Controls: DGPS/INS and Magnetic Markers, American Control Conference, p. 60-65, 2003.

3. J. Cheng, J. A. Farrell, L. Yu, E. Thomas, Aided Integer Ambiguity Resolution Algorithm, IEEE Position, Location, and Navigation Conference, 2004.

Additional publications concerning the experimental results from Crows Landing are expected.

References

[1] Abidin, H. Z., "New strategy for on-the-fly ambiguity resolution," *Proceedings ION GPS-91*, Sept. 1991.

[2] Bender, J., "An Overview of Systems Studies of Automated Highway Systems," *IEEE Trans. on Vehicular Technology*, Vol. 40 (1), pp. 82-99, 1991.

[3] J. Cheng, J. A. Farrell, L. Yu, E. Thomas, "Aided Integer Ambiguity Resolution Algorithm," IEEE Position, Location, and Navigation Conference, 2004.

[4] Counselman, C. C. and S. Gourevitch, "Miniature interferometer terminals for earth surveying: Ambiguity and multipath with global positioning system," *IEEE Transactions on Geoscience and Remote Sensing*, Oct. 1981.

[5] Cormier, W. and R. Fenton, "On the Steering of Automated Vehicles Velocity Adaptive Controller," *IEEE Trans. on Vehicular Technology*, Vol. 29, no.4, pp. 375-385, 1980.

[6] Dickmanns, E. and B. Mysliwetz, "Recursive 3-D road and relative ego-state recognition," *IEEE Transactions on Pattern Analysis and Machine Intelligence*, Vol. 14, pp. 199-213, 1992.

[7] Dunlay, R. T., "Obstacle avoidance perception processing for the autonomous land vehicle," in Proceedings of the IEEE International Conference on Robotics and Automation, pp. 912-917, 1987.

[8] Farrell, J. A. and M. Barth, *The Global Positioning System and Inertial Navigation*, McGraw-Hill (ISBN-0-07-022045-X), 1999.

[9] Farrell, J. A., T. Givargis. and M. Barth, "Real-time Differential Carrier Phase GPS-Aided INS," IEEE Transactions on Control Systems Technology. Vol. 8 (4), July 2000, pp. 709-721.

[10] Farrell, J. A. and M. Barth, "Integration of GPS-aided INS into AVCSS", California Path Research Report UCB-ITS-PRR-2000-22. August, 2000.

[11] Farrell, J. A., H.-S. Tan, and Y. Yang, "Carrier Phase GPS-aided INS based Vehicle Lateral Control," submitted ASME Journal of Dynamics Systems, Measurement, and Control, May 7, 2001, 39 m.s.

[12] Fenton, R., G. Melocik, and K. Olson, "On the Steering of Automated Vehicles: Theory and Experiment," *IEEE Transactions of Automatic Control*, Vol. 21, no.3, pp. 306-315, 1976.

[13] Fenton, R., and R. Mayhan, "Automated Highway Studies at The Ohio State UniversityAn Overview," *IEEE Trans. on Vehicular Technology*, Vol. 40, no.1, pp. 100-113, 1991.

[14] Frei, E. and G. Beutler, "Some considerations concerning an adaptive, optimized technique to resolve the initial phase ambiguities," *Proceedings of the Fifth International Geodetic Symposium on Satellite Positioning*, March 1989.

[15] Goad, C. C., "Robust techniques for determining gps phase ambiguities," *Proceedings of the sixth International Geodetic Symposium on Satellite Positioning*, 1992.

[16] Golub, G. H. and C. F. Van Loan, *Matrix Computations*, Johns Hopkins, Baltimore and London, 1996.

[17] Han, S. and C. Rizos, "Comparing gps ambiguity resolution techniques," *GPS World*, 1997.

[18] Hanson, A., E. Riseman, and C. Weems, "Progress in computer vision at the University of Massachusetts," in DARPA Image Understanding Workshop, pp. 39-47, 1993.

[19] Hatch, R. R., "Synergism of gps code and carrier measurements," *Proceedings of the Third International Geodetic Symposium on Satellite Doppler Positioning*, February, 1982.

[20] Hatch, R. R., "Dynamic differential gps at the centimeter level," *Proceedings of the Fourth International Geodetic Symposium on Satellite Positioning*, April, 1986.

[21] Hatch, R. R., "Instantaneous ambiguity resolution," *KIS-90 Symposium*, Aug. 1990.

[22] Hwang, P., "Kinematic gps: Resolving integer ambiguities on-the fly," *Proceedings IEEE PLANS*, March 1990.

[23] Kaplan, E. D., *Understanding GPS Principles And Applications*, Artech House Publisher, Boston, 1996.

[24] Kuan, Phipps, and Hsueh, "Autonomous Robotic Vehicle Road Following," *IEEE Transactions on Pattern Analysis and Machine Intelligence*, Vol. 10, pp. 648-658, 1988.

[25] Landau, H. and H.-J. Euler, "On-the-fly ambiguity resolution for precise differential positioning," *Proceedings ION GPS-92*, Sept. 1992.

[26] Mader, G. L., "Kinematic gps initialization using the ambiguity function," *Proceedings of the Sixth International Geodetic Symposium on Satellite Positioning*, March 1992.

[27] Mayhan, R. and R. Bishel, "A Two-Frequency Radar for Vehicle Automatic Lateral Control," *IEEE Trans. on Vehicular Technology*, Vol. 31, no.1, pp. 32-39, 1982.

[28] Masaki, I., Vision-Based Vehicle Guidance, New York: Springer-Verlag, 1992.

[29] Melbourne, W. G. "The case for ranging in gps-based geodetic systems," *Proceedings of the First International Symposium on Precise Positioning with GPS*, April, 1985.

[30] Remondi, B. W., "Pseudo-kinematic gps results using the ambiguity function method," *Navigation*, Spring.

[31] Schneidermann, H. and M. Nashman, "Visual processing for autonomous driving," in IEEE Workshop on Applications of Computer Vision, Palm Springs, CA, pp. 164-171, 1992.

[32] Shladover, S., et al., "Automatic Vehicle Control Developments in the PATH Program," *IEEE Trans. on Vehicular Technology*, Vol. 40, no.1, pp. 114-130, 1991.

[33] Sinko, J. W., "Single-epoch ambiguity resolution for highway and racetrack applications.," *Proceeding of ION GPS 2001*, Sept.2001.

[34] Teunissen, P. J. G., "A new method for fast carrier phase ambiguity estimation," *Proceedings of IEEE PLANS*, April 1994.

[35] Thorpe, C., et al, "Toward autonomous driving: the CMU Navlab", Part 1-Perception, *IEEE Expert*, Vol. 6, pp. 31-42, 1991.

[36] Yang, Y., J. A. Farrell, and H.-S. Tan, "Carrier Phase Differential GPS-aided INS based Vehicle Control: Experiement Results," Institue of Navigation, NTM 2001, Long Beach, 22-24 Jan. 2001.

[37] Yang, Y., J. A. Farrell, and H.-S. Tan, "GPS-aided INS based Control State Calculation for AHS," IEEE 2001 American Control Conference, June 2001.

[38] Yang, Y., R. T. Sharpe and R. R. Hatch, "A fast ambiguity resolution technique for rtk embedded within a gps receiver," *Proceeding of ION GPS 2002*, Sept.2002.

[39] Zhang, W., R. E. Parsons, and T. West, "An Intelligent Roadway Reference System for Vehicle Lateral Guidance/Control," Proceeding of the 1990 American Control Conference, San Diegp, CA, USA, 23-25 May 1990, pp.281-286.